JOURNAL OF GEOPHYSICAL RESEARCH, VOL. 108, NO. D22, 4708, doi:10.1029/2003JD003558, 2003

# Springtime trans-Pacific atmospheric transport from east Asia: A transit-time probability density function approach

Mark Holzer

Atmospheric Science Program, Department of Earth and Ocean Sciences, University of British Columbia, Vancouver, British Columbia, Canada

Physics Department, Langara College, Vancouver, British Columbia, Canada

Ian G. McKendry

Atmospheric Science Program, Department of Geography, University of British Columbia, Vancouver, British Columbia, Canada

Dan A. Jaffe

Interdisciplinary Arts and Sciences, University of Washington–Bothell, Bothell, Washington, USA

Received 3 March 2003; revised 4 July 2003; accepted 4 August 2003; published 29 November 2003.

[1] The atmosphere is known to episodically transport dust, aerosols, and gaseous pollutants from industrialized east Asia, the Gobi desert, and Siberian wild fires to western North America. We give a novel characterization of the climatological springtime transport from these regions and of the probability of transport "events," that is, long-range transport of high concentrations with minimal dispersion. Our primary transport diagnostic is the transit-time probability density function (pdf), $\mathcal{G}$, which is a tracer-independent measure of the flow that allows us to isolate the role of transport from other factors such as source variability and chemistry. The pdf approach, unlike typical back-trajectory analyses, captures transport due to all possible paths and accounts for both resolved advection and subgrid processes. We use a numerical model of the global atmosphere (Model of Atmospheric Transport and Chemistry (MATCH)) driven by National Centers for Environmental Prediction reananlysis data to establish the springtime statistics of daily averages of $\mathcal{G}$. A suitably defined average of $\mathcal{G}$ quantifies the climatological mass fraction of air from the source region per interval of transit times, or ages. Over the North American west coast, this fraction peaks at transit times of $\sim$8 days in the upper troposphere ($\sim$6 days later at the surface) for the dust and pollution regions and at 12–14 days for the Siberian region. An analysis of the variability of $\mathcal{G}$ at fixed transit time allows us to identify transport events and to estimate their probability of occurrence. This is illustrated for transport events to the "Pacific Northwest" (PNW) region of North America, defined as (43.8°–53.3°N) $\times$ (115.3°–124.7°W). Correlations between $\mathcal{G}$ averaged over the PNW and the winds at any point in the atmosphere identify large-scale anomaly structures of the flow that correspond to favorable transport to the PNW. *INDEX TERMS:* 0368 Atmospheric Composition and Structure: Troposphere—constituent transport and chemistry; 3309 Meteorology and Atmospheric Dynamics: Climatology (1620); 3367 Meteorology and Atmospheric Dynamics: Theoretical modeling; *KEYWORDS:* transit-time pdf, transport, troposphere

**Citation:** Holzer, M., I. G. McKendry, and D. A. Jaffe, Springtime trans-Pacific atmospheric transport from east Asia: A transit-time probability density function approach, *J. Geophys. Res.*, *108*(D22), 4708, doi:10.1029/2003JD003558, 2003.

## 1. Introduction

[2] A number of studies have documented long-range transport "events" from Asia to North America. During such events various combinations of dust, aerosols, and gaseous chemical pollutants are transported across the Pacific with minimal dispersion en route. Spectacular dust events have been observed from satellite, and the corresponding particle burdens have been measured over North America [e.g., *Merrill et al.*, 1989; *Husar et al.*, 2001; *McKendry et al.*, 2001; *Tratt et al.*, 2001; *Vaughan et al.*, 2001]. Such events have been explicitly modeled in detail [e.g., *Jaffe et al.*, 1999; *Hacker et al.*, 2001; *Uno et al.*, 2001; *Gong et al.*, 2003; *Jaeglé et al.*, 2003; *Zhao et al.*, 2003] with emphasis on matching simulations to observations. Less spectacular, but potentially more important, is the transport of chemical pollutants from the industrialized


0148-0227/03/2003JD003558$09.00

regions of east Asia. The Asian outflow of pollutants has been the focus of the February–April 2001 TRACE-P aircraft mission (for an overview, see *Jacob et al.* [2003]), and the trans-Pacific transport of these pollutants can also occur episodically [*Yienger et al.*, 2000; *Jaffe et al.*, 2001, 2003; *Price et al.*, 2003; *Heald et al.*, 2003]. While dust transport events to North America usually also carry pollution, pollution and dust events need not coincide since they come from physically separate sources. There have also been measurements over western North America of chemical species associated with biomass burning with possible origins in the wild fires of Siberia [*Jaffe et al.*, 2001; *Kajii et al.*, 2002; I. Bertschi et al., manuscript in preparation, 2003].

[3] Observed transport events are episodic in nature for several reasons. For some species such as dust, the source itself is episodic (soil has to be very dry and a storm has to inject the dust into the boundary layer) [e.g., *Prospero et al.*, 2002; *Zhao et al.*, 2003]. Similarly, wild fires do not burn constantly or with steady intensity. For industrial pollutants, however, the source is only slowly varying and a long-range transport event occurs if the flow allows transport with minimal dispersion and limited chemical destruction of the species. In addition to these episodic events, Asian pollutants are constantly transported in lesser concentrations to North America, where they contribute to the ever-present background pollution [*Berntsen et al.*, 1999; *Jacob et al.*, 1999]. Actual tracer mixing ratios of specific species are determined by the combined effects of transport, source variability, and chemical processing. Our aim here is to isolate the role of transport from all the other factors.

[4] In this work we do not model transport events for specific gases and particulates. Instead, we address statistical questions: What is the climatological transport of air after it has had contact with the source regions of interest? What constitutes a transport "event" and how likely are these? What features of atmospheric flow result in particularly effective transport from east Asia to North America? To help us answer these questions, we focus on the transit-time probability density function (pdf), $\mathcal{G}$, which is a tracer-independent transport diagnostic [*Hall and Plumb*, 1994; *Holzer and Hall*, 2000]. This approach has strong advantages over trajectory analyses, because it accounts for all possible paths from the source region to any point in the atmosphere. The transit-time approach takes advantage of an atmospheric transport model's full transport operator including parameterized small-scale transport usually ignored in trajectory analyses. Trajectory analyses typically cannot quantify dilution because of entrainment and mixing en route, processes that are naturally built into $\mathcal{G}$. The pertinent properties of $\mathcal{G}$ are summarized in the following section.

## 2. Transit-Time pdf

[5] The transit-time pdf, $\mathcal{G}$, is defined so that $\mathcal{G}(\mathbf{r}, t|\Omega, t')dt'$ is the mass fraction of an air parcel at point $\mathbf{r}$ and time $t$ that had last contact with a specified surface, $\Omega$, during the time interval between times $t'$ and $t' + dt'$. An example of a contact surface, $\Omega$, that we will be interested in is the land surface of industrialized east Asia. If we imagine a macroscopic parcel of air as being composed of microscopic fluid elements that keep their identity over the timescales of interest, or "particles" for short, then $\mathcal{G}(\mathbf{r}, t|\Omega, t')dt'$ is the mass fraction of particles that had a transit time between $t - t'$ and $t - t' + dt'$ to travel from $\Omega$ to $\mathbf{r}$.

[6] If all the particles traveled along a single trajectory of length $L$ at average speed $v$, then $\mathcal{G}$ would be a delta function peaked at $L/v$, that is, we would have $\mathcal{G} = \delta(t - t' - L/v)$, where $\delta(\ldots)$ is the Dirac delta function. Atmospheric transport is, of course, much more complex than a conveyor belt along a single trajectory. The transit-time pdf is not sharply peaked but typically very broad reflecting the fact that the particles of $\Omega$ origin in a given air parcel will have taken an infinity of different paths through the fluid. Transit along some paths is rapid, along others it is slow. Borrowing from the vocabulary of mathematical physics, we refer to $t$ as the "field time," and to $t'$, as the "source time." It is important to note that generally $\mathcal{G}$ has separate dependencies on $t$ and $t'$. Only for stationary flow is $\mathcal{G}$ a function of transit time, $t - t'$, only.

[7] It is straightforward to calculate $\mathcal{G}$ as the mixing ratio of a synthetic passive tracer subject to special boundary conditions (BCs) [*Hall and Plumb*, 1994; *Holzer and Hall*, 2000]. The pdf, $\mathcal{G}$, obeys the passive-tracer transport equation

$$\frac{\partial}{\partial t}\mathcal{G}(\mathbf{r}, t|\Omega, t') + \mathcal{T}(\mathcal{G}(\mathbf{r}, t|\Omega, t')) = 0, \tag{1}$$

which has no explicit sources (zero right-hand side), and where $\mathcal{T}$ is the linear transport operator representing the advective-diffusive flow of the atmosphere (some form of diffusion is always necessary to model the pseudo-random nature of the flow on the smallest resolved scales [e.g., *Hall and Holzer*, 2003]). Equation (1) is solved subject to the boundary condition (BC)

$$\mathcal{G}(\mathbf{r}, t|\Omega, t') = \delta(t - t'), \tag{2}$$

for $\mathbf{r}$ on $\Omega$. On all other boundaries, $\mathcal{G}$ is subject to the natural zero-flux BCs of the fluid domain. Note that $\mathcal{G}(\mathbf{r}, t|\Omega, t') = 0$ for $t < t'$ since there cannot be a response before the pulse has occurred. The $\delta$-function BC of equation (2) labels, or "marks," fluid elements that make contact with $\Omega$ at $t = t'$ with the tracer $\mathcal{G}$. Marked fluid elements retain their marking until they make contact with $\Omega$ again, when they lose their marking since the BC of equation (2) sets $\mathcal{G}$ to zero on $\Omega$ for $t > t'$.

[8] If one goes back infinitely far in time, one can be certain that every fluid element comprising an air parcel will have had $\Omega$ contact. Consequently, the mass fraction of air that had contact with $\Omega$ at any time in the past must be unity, that is, $\mathcal{G}$ is properly normalized with

$$\int_{-\infty}^{t} dt' \mathcal{G}(\mathbf{r}, t|\Omega, t') = 1. \tag{3}$$

Note that the integral of equation (3) is performed over source time, $t'$, at fixed field time, $t$. While it may be tempting to interpret $\mathcal{G}$ as a function of $t$ (for a given pulse at $t'$) as a transit-time pdf, this would be correct only for stationary flow. For stationary flow, $\mathcal{G}$ depends on $t$ and $t'$ through $t - t'$ only, so that one can switch integration variables and replace the integral of equation (3) with $\int_{t'}^{\infty} dt \mathcal{G}(\mathbf{r}, t|\Omega, t')$. However, on the timescales considered

here, atmospheric flow is highly nonstationary, so that one must use equation (3).

[9] A very useful property of $\mathcal{G}$ is that it is a propagator of time-dependent BCs for mixing ratio on $\Omega$, provided these are spatially uniform over $\Omega$. Given a time series $\chi_\Omega(t')$ for mixing ratio on $\Omega$, the mixing ratio at any other point $\mathbf{r}$ in the atmosphere (the "response" to $\chi_\Omega$) can then be obtained from the convolution

$$\chi(\mathbf{r},t) = \int_{-\infty}^{t} dt' \mathcal{G}(\mathbf{r},t|\Omega,t')\chi_\Omega(t'). \quad (4)$$

Finally, $\mathcal{G}$ is intimately connected to the Green function of the transport operator, which provides a general framework for the analysis of $\mathcal{G}$ [*Holzer and Hall*, 2000] (see, e.g., *Morse and Feshbach* [1953] for a general treatise on Green functions).

## 3. Numerical Calculations of $\mathcal{G}$

[10] To compute the transit-time pdf, $\mathcal{G}$, we use the Model of Atmospheric Transport and Chemistry (MATCH), a three-dimensional global model of the atmosphere developed by *Rasch et al.* [1997]. MATCH uses the mass-conserving Split Implementation of Transport Using Flux Integral Representation (SPITFIRE) flux algorithm [*Rasch and Lawrence*, 1998]. MATCH has the same kind of parameterizations for sub-grid processes as state-of-the-art general circulation models (GCMs), such as convection and boundary-layer mixing. However, MATCH is an "off-line" model that does not integrate prognostic momentum equations, but instead uses predefined winds and BCs as may be obtained from observational analyses or GCMs. We drive MATCH with the reanalysis data from the National Centers for Environmental Prediction (NCEP) [*Kalnay et al.*, 1996; *Kistler et al.*, 2001] and run MATCH at the resolution of the T63 NCEP data: a Gaussian grid of 94 latitudes and 192 longitudes ($\sim$1.9° × 1.9°), with 28 hybrid levels up to $\sim$3 mb.

[11] For our choice of contact surfaces, $\Omega$, limited computational resources make it impractical to be comprehensive in covering all Asian surface regions where air may be labeled with measurable tracers. We therefore limit our focus to transport from three contact surfaces in east Asia that approximately coincide with sources of measurable tracers of particular interest to the central west coast of North America. (a) The "pollution region," $\Omega_P$: This region was chosen to approximate the surface area of east Asia with the heaviest industrial pollution. As a proxy for such pollution, we considered $SO_2$ emissions. However, we emphasize that it is not our aim to produce a contact region that represents an accurate map of $SO_2$ emissions. Instead, we merely wish to identify a region of east Asia where boundary-layer air is likely to be injected with pollutants. Accordingly, we base our choice of $\Omega_P$ only loosely on the 1° × 1° $SO_2$ inventory of *Benkovitz et al.* [1996] according to the following rules, which are arbitrary, but which allow an objective definition of $\Omega_P$ and to which the choice of region is not very sensitive: Inventory grid points with emissions above 1000 kg/yr/grid point (the units of the data set) are included, the resulting field is area averaged to the MATCH grid, we limit to 20–44°N, east of 100°E, and "holes" in the resulting $\Omega$ are "filled in." (b) The "dust region," $\Omega_D$: This is the region where boundary-layer air is potentially labeled by desert dust. We define $\Omega_D$ as the bare land whose elevation is below 3 km as determined from the NDVI-derived land-cover data set prepared by *DeFries and Townshend* [1994]. (c) The "fire region," $\Omega_F$: Finally, to investigate the transport of air from Siberia which could potentially be labeled by a chemical bio-mass-burning signature, we chose for $\Omega_F$ the land surface contained in (45.7–61.0°N) ×(125–140°E). Most large springtime fires are observed in this area, which accounted for 90% of the total emissions from fires in 1998 [*Kajii et al.*, 2002]. Figure 1a shows all three regions on the MATCH grid. All $\Omega$ lie on the model's land surface; ocean points have been excluded. The areas, $A$, of the source regions are $A(\Omega_P) = 3.74 \times 10^6$ km$^2$, $A(\Omega_D) = 1.63 \times 10^6$ km$^2$, and $A(\Omega_F) = 1.60 \times 10^6$ km$^2$. The corresponding mean elevations, $h$, are $h(\Omega_P) = 696$ m, $h(\Omega_D) = 1562$ m, and $h(\Omega_F) = 497$ m.

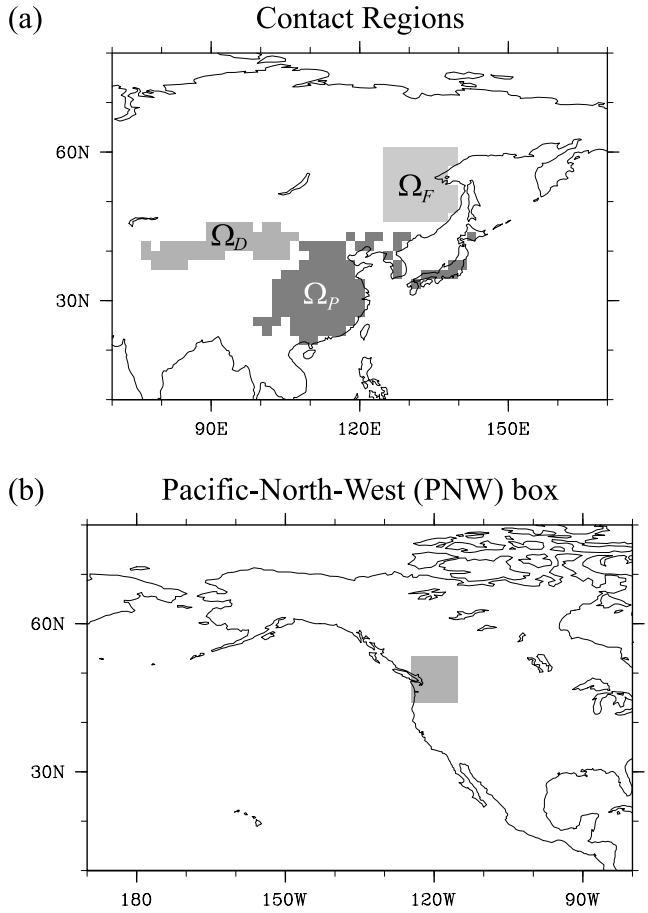


**Figure 1.** (a) The three contact regions defined here: $\Omega_P$ is the region of east Asia where air is likely to be labeled with pollution. $\Omega_D$ is a desert region possibly labeling air with dust particles. $\Omega_F$ is the region where air is potentially labeled with a chemical bio-mass-burning (fire) signature. (b) The Pacific Northwest (PNW) box defined as (43.8°–53.3°N) × (115.3°–124.7°W) used to average $\mathcal{G}$ for more robust field-point statistics.

[12] Several comments about our choices for $\Omega$ are in order. Southeast (SE) Asia is well known to be a significant

source of springtime biomass burning [e.g., *Duncan et al.*, 2003]. However, we excluded SE Asia from consideration here not only because of computational limitations, but also because observational studies suggest that direct transport from SE Asia to the central west coast of North America is rare [*Jaffe et al.*, 2001]. While our choice of $\Omega_F$ is motivated by trying to understand the transport of air that is potentially labeled by biomass burning, we acknowledge that the small-scale flow associated with fires, such as buoyancy-driven updrafts over hot spots, will not be captured by the MATCH transport operator. We make no attempt here to parameterize fire processes, and treat $\Omega_F$ on the same footing as $\Omega_P$ and $\Omega_D$. Sensitivity to missing fire processes is further discussed in section 5.

[13] We emphasize that the contact regions, $\Omega$, are not used as emission sources for actual trace species. It is not our aim here to simulate tracers characteristic of biomass burning, industrial pollution, or dust. Instead, we use the $\Omega$ regions to compute $\mathcal{G}$, the pdf of transit times since fluid elements had last contact with these regions. (The synthetic tracers employed to calculate $\mathcal{G}$ are also not injected with any predetermined emission fluxes, but instead are constrained to satisfy pulse boundary conditions on mixing ratio; see section 2 or, for more detail, *Holzer and Hall* [2000].) The pdf $\mathcal{G}$ is a tracer-independent diagnostic of the transport of fluid elements from $\Omega$ regardless of whether they are labeled with measurable tracers. We are thus able to isolate the role of transport from any other factors influencing the mixing ratios of particular trace species.

[14] For a given contact region, $\Omega$, we now compute $\mathcal{G}$ as follows. The delta-function of equation (2) is broadened to a day-long, 00Z to 00Z, square pulse of amplitude 1/day. The response to such a broadened pulse gives us $\mathcal{G}$ coarse grained in time, that is, convolved with the one-day square pulse [*Holzer*, 1999]. Consequently, all the time integrals of section 2 can be evaluated as sums, where the source time $t'$ is now a discrete index labeling the day during which the square pulse is ''on'' (nonzero). The pulse BC is enforced by setting the mixing ratio for $\Omega$ grid points on the lowest model level to unity while the pulse in on, and to zero when the pulse is off. Elsewhere on the Earth's surface, and at the top of the atmosphere, zero-flux BCs are maintained. We choose day-long pulses so that day-to-day variability is resolved (transport events evolve over a few days). Longer pulses (say week-long) were not used because this would make comparison with observed transport events over North America very difficult if not impossible, even though synoptic variability might be captured.

[15] To establish the springtime climate of $\mathcal{G}$ for a given $\Omega$, we compute $\mathcal{G}(\mathbf{r}, t|\Omega, t')$ for the source days $t'$ of 21 March to 10 May for the years 1997 to 2001, inclusive. This gives us 51 realizations of $\mathcal{G}$ per spring for 5 years. We compute the evolution of each $\mathcal{G}$ until $t - t'$ is at least 30 days, and archive daily averages of $\mathcal{G}$ and the corresponding meteorological fields.

## 4. Structure of $\mathcal{G}$ in the $t - t'$ Plane

[16] To clarify the interpretation of $\mathcal{G}$ as a pdf, we consider the structure of $\mathcal{G}$ as a function of source and field times, at some fixed location. Instead of picking a single grid point, we reduce the variability of $\mathcal{G}$ by averaging over the box defined by (43.8°–53.3°N) × (115.3°–124.7°W). For lack of a better term we refer to this region as the ''Pacific Northwest'' (PNW), acknowledging that it includes not only Washington State, northern Oregon, and parts of Idaho, but also southern British Columbia and a small part of Alberta in the Canadian South West. This region is shown in Figure 1b, and we denote averages over it by $[\ldots]_{PNW}$. (For a more robust comparison with observations, $[\mathcal{G}]_{PNW}$ is also considered in sections 6 and 7, where we also discuss sensitivities to the definition of the PNW field-point region.)

[17] Figure 2 shows $[\mathcal{G}(\mathbf{r}, t|\Omega_P, t')]_{PNW}$ at 500 mb as a function of $t$ and $t'$ for spring 1998. Horizontal slices through this data (i.e., slices at fixed source time, $t'$) shown in Figure 2b correspond to the time-evolving response to a one-day square pulse on $\Omega_P$ that occurred at source time $t'$. This is what is directly computed in our simulations. The area under these curves is in general not fixed, but varies for different $t'$ and with distance from $\Omega_P$. Vertical slices at fixed field time, $t$, shown in Figure 2c correspond to the mass fraction of air at $t$ that had last contact with $\Omega_P$ during day $t'$, as a function of $t'$. These curves are the transit-time pdfs for transit time $\xi \equiv t - t'$. The integration in the normalization of equation (3) corresponds to summing vertically in Figure 2c at fixed $t$ from $-\infty$ to the line $t = t'$. As a check on the numerics this was explicitly verified closer to the source, where there is negligible weight under the tail for $\xi > 30$ days.

[18] The structure of $\mathcal{G}$ in the $t - t'$ plane (Figure 2) shows several characteristic timescales. The shortest timescale is the minimum time required for air to get from $\Omega_P$ to the PNW box: ~4 days at 500 mb. Then $\mathcal{G}$ peaks at the most probable transit time (between ~5–10 days at 500 mb), when a parcel at the field point has the largest fraction of $\Omega$ air of transit times, or ''ages,'' in the interval $(\xi, \xi + \Delta t')$, where $\Delta t' = 1$ day. The peak then slowly decays as the response to the initial delta-function pulse is first mixed zonally and then, on longer timescales not visible in the figure, over the hemisphere, and eventually between hemispheres. Every time a fluid element makes contact again with $\Omega$ it loses its marker by virtue of the BCs so that we are guaranteed that $\mathcal{G}$ eventually decays to zero. The closer one is to $\Omega$, the sharper the peak becomes, and the less area lies under the decaying tail, with $\mathcal{G}$ being a perfect square pulse on $\Omega$ itself.

[19] Figures 2a–2c show that there is considerable daily variability in the evolution of $\mathcal{G}$, even when area-averaged over the PNW box. The large peak in $\mathcal{G}$ visible at field time $t = 36$ days (26 April) and source time $t' = 30$ days (20 April) coincides with the well-documented 1998 transport event [*Husar et al.*, 2001]. This peak represents the mass fraction of $\Omega_P$ air over the PNW at 500 mb on 26 April that had a transit time of $\xi = t - t'$ between 5 and 6 days. The vertical slice of Figure 2c at $t = 36$ days gives the fractions of $\Omega_P$ air on 26 April that had contact with $\Omega_P$ during the days $t'$ from $t' = t$ on backward in time (downward on the graph). Before returning to an analysis of such events, the following section quantifies the climatological average behavior of $\mathcal{G}$.

## 5. Transit-Time "Climate"

[20] The climatological mean springtime transit-time pdf from a given contact region is naturally defined as the

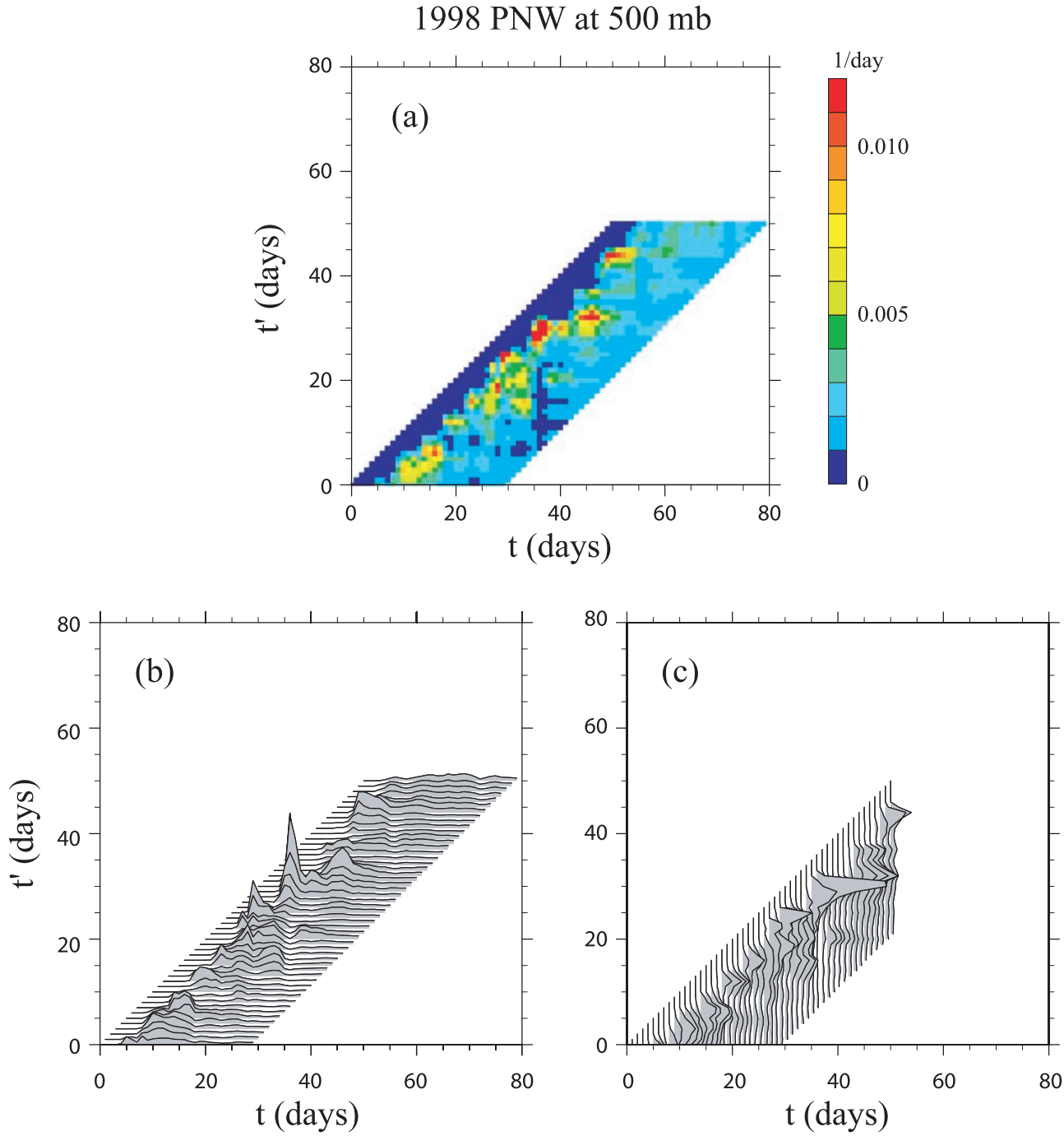


**Figure 2.** $[\mathcal{G}(\mathbf{r}, t|\Omega_P, t')]_{PNW}$ at 500 mb for $t' = 21$ March to 10 May 1998. (a) A density plot of the daily averages of $[\mathcal{G}]_{PNW}$ in the $(t, t')$-plane. ($[\mathcal{G}]_{PNW}$ is shown only for transit times $t - t' \leq 30$ days.) (b) $\mathcal{G}$ as a function of transit time at fixed source time $t'$ (horizontal cuts through Figure 2a). This shows $\mathcal{G}$ as actually computed: The tracer response to a pulse BC during day $t'$. These curves are, however, not normalized transit-time pdfs. (c) $\mathcal{G}$ as a function of $t - t'$ at fixed field time $t$ (vertical cuts through Figure 2a). These curves are the normalized transit-time pdfs.

average response to the δ-function BC, averaged over source-region pulse times $t'$ at fixed transit time ξ. For example, to obtain the 1998 average for the PNW region at 500 mb, we horizontally shift the curves of Figure 2b to a common origin and average them together. Thus we define the 5-year, springtime climatological average $\langle\mathcal{G}\rangle$ by

$$\langle\mathcal{G}(\mathbf{r}, \xi, \Omega)\rangle = \frac{1}{5}\sum_{n=1}^{5}\frac{1}{T}\int_{t_{0n}}^{t_{0n}+T} dt'\mathcal{G}(\mathbf{r}, \xi + t'|\Omega, t'), \qquad (5)$$

where $T = 51$ days and $t_{0n}$ is 21 March of the $n$th year. (In practice the $t'$ integral of equation (5) is performed as a sum over the 51 source days.) One could argue that a more

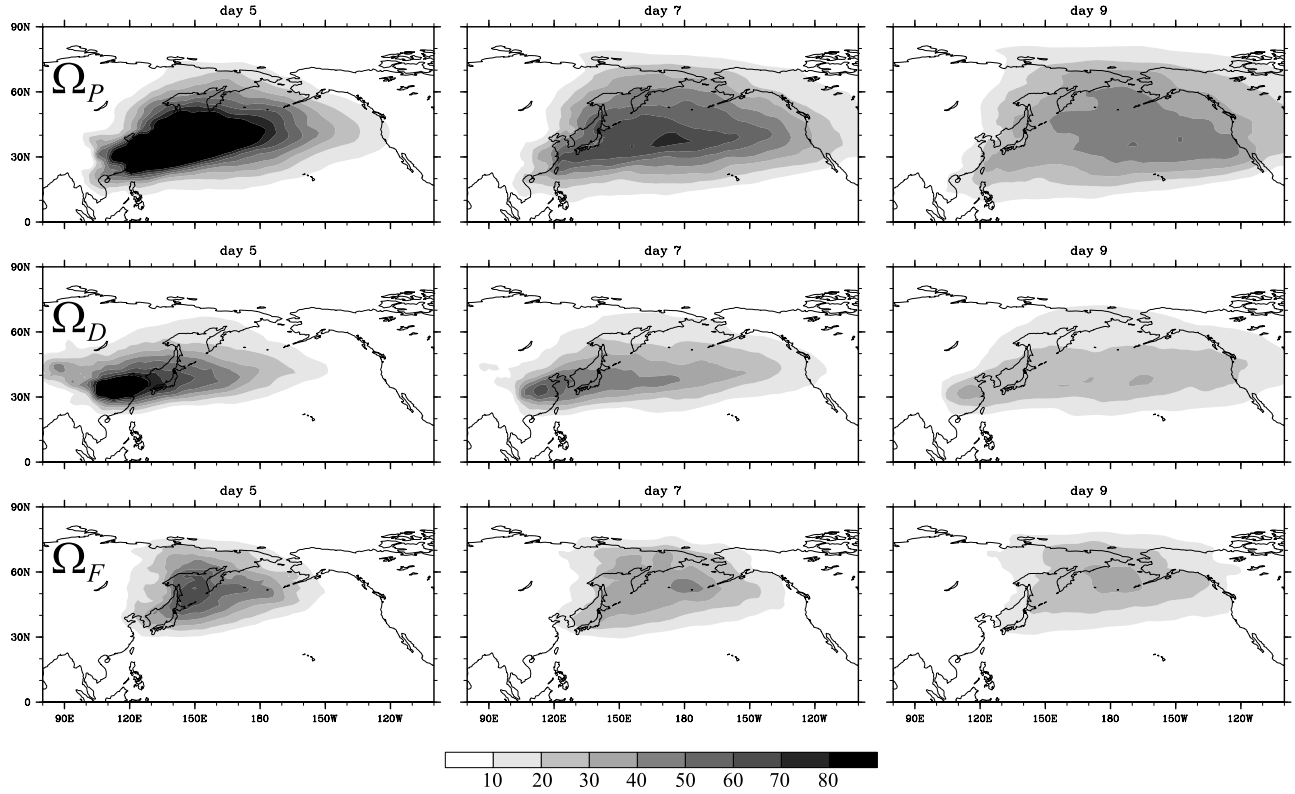


**Figure 3.** Springtime ensemble average of the vertically integrated pdf, $\langle\widetilde{\mathcal{G}}(\xi)\rangle$, in units of kg m$^{-2}$ day$^{-1}$ for transit times $\xi$ = 5, 7, and 9 days.

natural ensemble average would be obtained by shifting the curves of Figure 2c vertically to a common origin so that normalized pdfs are averaged together. However, as long as transport is statistically stationary during spring, this ensemble average and that of equation (5) are equivalent. We assume such stationarity and use equation (5).

[21] To characterize the climatological mean state of $\mathcal{G}$ for each contact region, $\Omega$, Figure 3 shows maps of the ensemble averaged vertical integral, or "burden," $\langle\tilde{\mathcal{G}}\rangle$, as it evolves with transit time, $\xi$, from $\xi$ = 5 to 9 days, where $\tilde{\mathcal{G}} \equiv \int_0^{p_s} \mathcal{G} dp/g$ ($p$ is pressure, $p_s$, surface pressure, and $g$, the acceleration of gravity). The southern flanks of the "plumes" of $\langle\tilde{\mathcal{G}}\rangle$ for $\Omega_P$ and $\Omega_D$ have relatively sharp meridional gradients indicating low variability and weak mixing there, while the northern flanks of the $\Omega_P$ and $\Omega_D$ plumes, and the entire $\Omega_F$ plume, are more diffuse in the region of midlatitude baroclinic eddies. The Northern Hemisphere (NH) average of $\langle\tilde{\mathcal{G}}\rangle$ at $\xi$ = 5 days is, in units of kg m$^{-2}$ day$^{-1}$, 11.7 for $\Omega_P$, 5.55 for $\Omega_D$, and 3.49 for $\Omega_F$. For small transit times and a given area of $\Omega$, the NH average of $\langle\tilde{\mathcal{G}}\rangle$ gives an indication of how effective fluid elements are in escaping the lowest model layer over $\Omega$ while the source pulse is on, and how successful they are at avoiding contact with $\Omega$ after the source pulse is off ($G$ is conserved in the interior of the atmosphere). Although one expects a difference in the pdfs solely from the fact that the $\Omega$ have different areas (the larger the area, the larger the initial burdens, and the more rapid the ultimate long-time decay), the contact area is clearly not the factor distinguishing the $\Omega_D$ and $\Omega_F$ cases for which this area is almost the same. Figure 4 displays NH meridional averages of $\langle\mathcal{G}\rangle$ to show the evolution of the vertical structure of the pdfs as $\xi$ increases from 5 to 15 days. As a summary of characteristic transit times, we consider the peak time of the climatological pdf, that is, the time for which $\langle\mathcal{G}\rangle$ reaches its maximum value at a given location (this is also the most probable transit time to that location). Note that, unlike $\langle\mathcal{G}\rangle$ itself, the peak time has virtually no dependence on the area of $\Omega$. Figure 5 shows maps of the peak time of $\langle\tilde{\mathcal{G}}\rangle$, and Figures 6a–6c show the vertical structure of the peak time of $\langle\mathcal{G}\rangle$ in zonal and meridional cross-sections at 45°N and 124°W, respectively.

[22] Figures 3–6 show that the $\Omega_P$ and $\Omega_D$ cases have qualitatively similar transport, while the $\Omega_F$ case is distinct from both with considerably weaker transport. On average, after air makes contact with either $\Omega_P$ or $\Omega_D$ it rapidly accesses the upper troposphere, where it is then efficiently transported by flow dominated by the jet streams. Although the detailed mechanisms of the ascend into the free troposphere are not our focus here, frontal lifting in "warm conveyor belts" [*Stohl*, 2001] was observed to be the dominant mechanism during the TRACE-P mission [e.g., *Heald et al.*, 2003; *Jacob et al.*, 2003]. Over western North America at ~124°W, the climatological $\Omega_P$ and $\Omega_D$ transit-time pdfs first peak in the upper atmosphere at ~300 mb, ~45°N after a transit time of ~8 days (Figures 6a and 6b). In contrast, $\Omega_F$ air is primarily transported in the middle to lower troposphere and has a much higher probability of making renewed $\Omega$ contact after short transit times. This is evident from Figure 4, and consistent with the smaller NH average burdens, the much smaller zonal extent of the $\Omega_F$ plume for a given transit

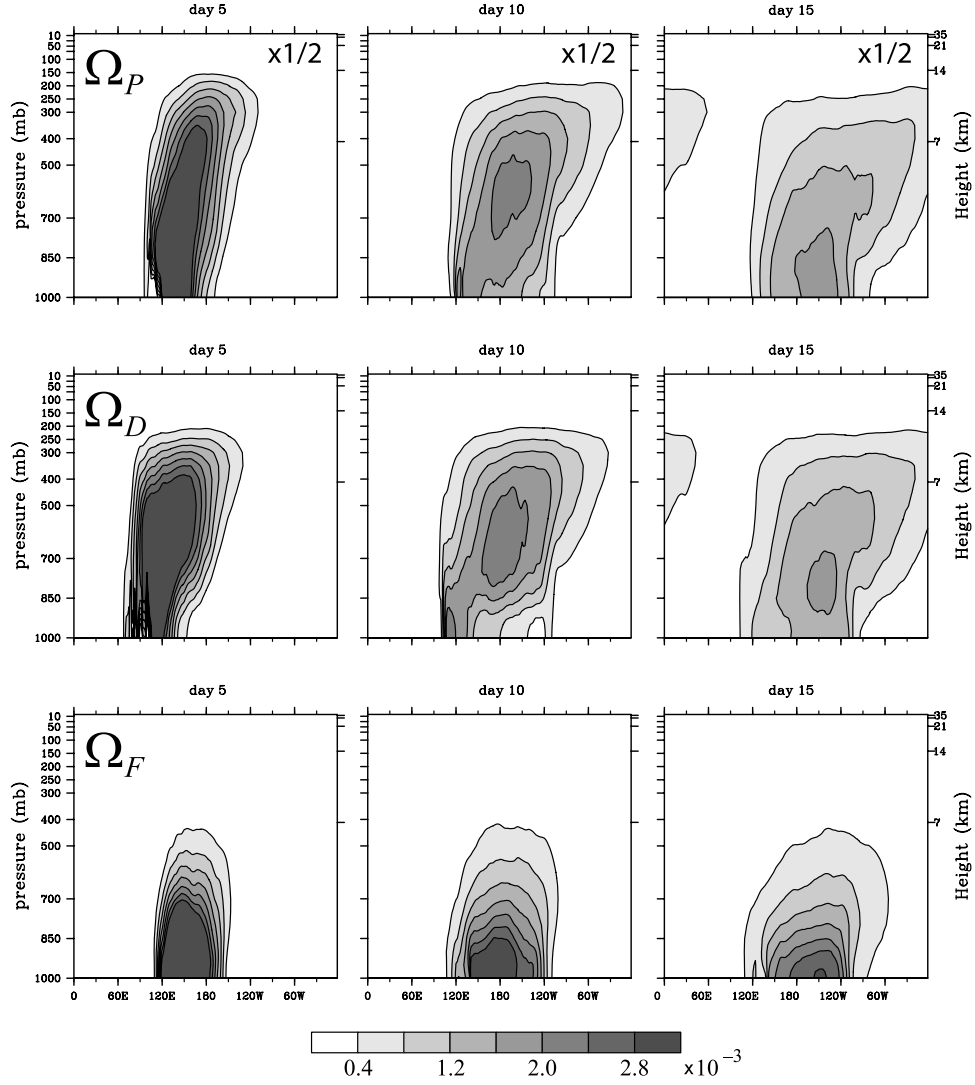


**Figure 4.** Springtime NH meridionally and ensemble averaged pdf, $\langle \mathcal{G}(\xi) \rangle$, in units of day$^{-1}$ for transit times $\xi$ = 5, 10, and 15 days. The values for the $\Omega_P$ case were multiplied by 1/2 before contouring.

time (Figure 3), and longer minimum peak times at ~124°W of ~12 days, with weak vertical gradients (Figure 6c). The $\Omega_F$ patch sits in a region of frequent springtime subsidence over the Siberian High, which means that air that contacts $\Omega_F$ will have relatively less chance to be transported away before making renewed $\Omega_F$ contact. Consequently, long transit times and corresponding long-range transport are relatively rare. Furthermore, $\Omega_F$-air that does escape $\Omega_F$ is not injected into vigorous zonal flow dominated by jet streams, but instead gets caught in more eddy-dominated high-latitude flow.

[23] As mentioned in section 3, the NCEP-reanalysis-based MATCH transport operator does not contain the buoyancy-driven flow generated by forest fires. For the $\Omega_F$ case the question therefore arises: Does air lofted by fire, and potentially labeled by pollutants such as carbon monoxide (CO), undergo transport qualitatively different from that of surface air? In fact, studies that explicitly model the transport of CO from boreal forest fires assume an effective injection height between 500 and 3000 m [*Wotawa and Trainer*, 2000]. In an attempt to bound the effect of such lofting, we compared the pdf since last surface contact, $\mathcal{G}$, to the pdf since last volume contact, $\mathcal{G}_V$, for a ~3000 m-thick volume over $\Omega_F$ for April 2001 (not shown). We define $\mathcal{G}_V$ as the response to the pulse condition (2) applied throughout the volume. While $\mathcal{G}_V$ has ~6 times the amplitude of $\mathcal{G}$, the mean structure of $\mathcal{G}_V$ shows transport that is qualitatively very similar to that of $\mathcal{G}$, seen in Figure 4. Fluid elements from the 3000 m-thick volume are still found primarily close to the surface in the lower troposphere as they travel east. There are episodes when $\mathcal{G}_V$, and also $\mathcal{G}$, have significant amplitude above ~500 mb. For such cases, air is often transported rapidly to the arctic, where $\mathcal{G}_V$ and $\mathcal{G}$ peak at ~124°W between 4 and 8 days. However, at least for $\mathcal{G}$, these episodes average out in the 5-year springtime mean and therefore do not appear in the peak times of Figure 6c. While individual fire events may loft air so it can be transported rapidly, the climatological mean transport would not likely be qualitatively different if fires were explicitly parameterized into the transport operator.

[24] Although transport of $\Omega_P$ and $\Omega_D$ air to western North America is rapid in the upper troposphere, at the

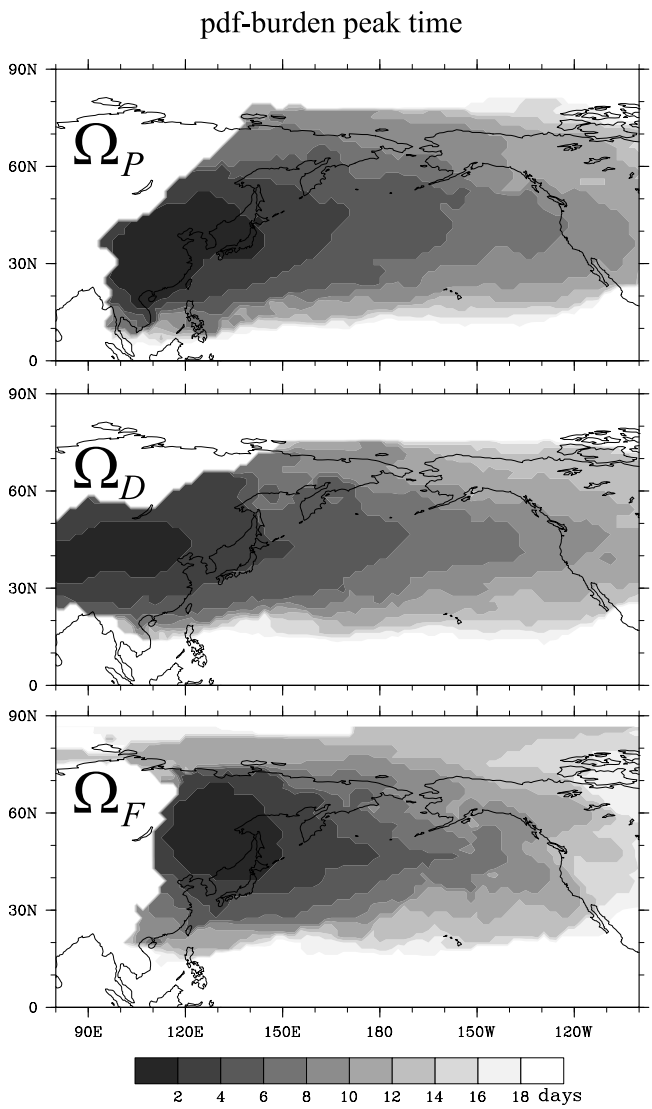


**Figure 5.** Peak time in days of the springtime average of the vertically integrated pdf, $\langle \widetilde{\mathcal{G}}(\xi) \rangle$.

Earth's surface the $\Omega_P$ and $\Omega_D$ transit-time pdfs do not peak until $\xi \sim 14$ to 16 days. This is comparable to the ~12 to 14 days required for the average $\Omega_F$ transit-time pdf to peak at the surface along the west coast of North America. Thus, as far as bringing $\Omega$ air to the surface is concerned, the more sluggish transport of $\Omega_F$ air throughout the middle to lower troposphere is of similar efficiency as the more rapid upper tropospheric transport of $\Omega_P$ and $\Omega_D$ air followed by vertical downward transport as seen in Figure 4 (at least as modeled with MATCH's partially parameterized vertical processes).

[25] The peak times of $\langle \mathcal{G} \rangle$ calculated here are in broad agreement with the transit-time estimates of *Kotchenruther et al.* [2001]. Using propane/ethane and ethyne/CO ratios measured from near the surface to 8-km altitude, *Kotchenruther et al.* [2001] estimate the spring 1999, east-Asia-to-PNW average transit time to be 8–10 days for a WNW-flow regime, and 16–20 days for a SW-flow regime.

[26] The climatological mass fraction of air that had last contact with $\Omega$ at any time in the past is unity as expressed by equation (3) and therefore not of interest. However, if air is literally labeled at $\Omega$ with an exponentially decaying chemical pollutant, such as light hydrocarbons undergoing oxidation with hydroxyl radical (OH) [see, e.g., *Ehhalt et al.*, 1998; *Kotchenruther et al.*, 2001], it is useful to quantify the mass faction of a given air parcel that carries this chemical signature. If the chemical decay time constant is $\tau_c$, then this fraction is given by

$$f(\mathbf{r}, t|\Omega, \tau_c) \equiv \int_0^\infty d\xi e^{-\xi/\tau_c} \mathcal{G}(\mathbf{r}, t|\Omega, t-\xi). \tag{6}$$

Note that as $\tau_c \to \infty$, $f \to 1$. Figure 7 shows $f$ ensemble averaged at 850 mb for a pollutant with $\tau_c = 6$ days. The climatological, springtime, near-surface mass fractions of air labeled by such a pollutant from east Asia ($\Omega_P$) can be seen to be on the order of 5 parts per thousand over western North America. If such a chemical pollutant has a time-independent source-region mixing ratio, $\chi_\Omega$, then its mixing ratio at ($\mathbf{r}$, $t$) is given by $\chi(\mathbf{r}, t) = f(\mathbf{r}, t|\Omega, \tau_c)\ \chi_\Omega$ from equation (4).

## 6. Probability and Identification of Transport Events

[27] Here we ask whether the fraction of air at ($\mathbf{r}$, $t$) that has last been in contact with $\Omega$ at any time during the previous $\tau$ days, is unusually high. We can think of this fraction as $\Omega$ air with transit times $\xi \leq \tau$ or, equivalently, as $\Omega$ air "aged" $\tau$ or less. If this $\Omega$-air fraction is unusually high, as determined from its sample distribution, then we can say that there has been an $\Omega$-to-$\mathbf{r}$ transport "event" at ($\mathbf{r}$, $t$). The fraction of $\Omega$ air "aged" $\tau$ or less is given by

$$g(\mathbf{r}, t|\Omega, \tau) \equiv \int_0^\tau d\xi \mathcal{G}(\mathbf{r}, t|\Omega, t-\xi). \tag{7}$$

The fraction $g$ is closely related to the fraction $f$ defined in equation (6), but the integral of equation (7) has the advantage of guaranteed convergence for the finite-duration runs analyzed here. One could also simply ask whether $\mathcal{G}$ for a fixed transit time, $\xi$, is unusually large. However, we use $g$ instead since this integrated variable has more robust statistics and a simple physical interpretation.

[28] To quantify whether $g$ is unusually large, we focus for economy of analysis on the PNW region (Figure 1b), integrate vertically, and average over this region to obtain $[\widetilde{g}]_{PNW}$. The daily values of $[\widetilde{g}]_{PNW}$ are available for 51-$\tau$ days of every spring (1997–2001) giving a sample size of $N = 255 - 5\tau$. Sorting these values allows us to identify for which days $[\widetilde{g}]_{PNW}$ lies above the 90th percentile of its sample distribution, giving us an objective, quantitative measure of when air in the PNW region is unusually rich in $\Omega$ air. The days above the 90th percentile therefore identify transport events which, by construction, are responsible for 10% of the $\Omega$-air of age $\tau$ or less that resides in the PNW box during spring.

[29] Figures 8a–8c show the dates of field times, $t$, for which $[\widetilde{g}]_{PNW}$ lies above its 90th percentile for the three choices of $\Omega$ and with values of $\tau$ from 4 to 12 days. Well-known transport events are readily identified. For example, the day with the highest $\Omega_P$ burden aged 8 days or less ($\tau = 8$ days) was 26 April 1998 (Figure 8a). The recent

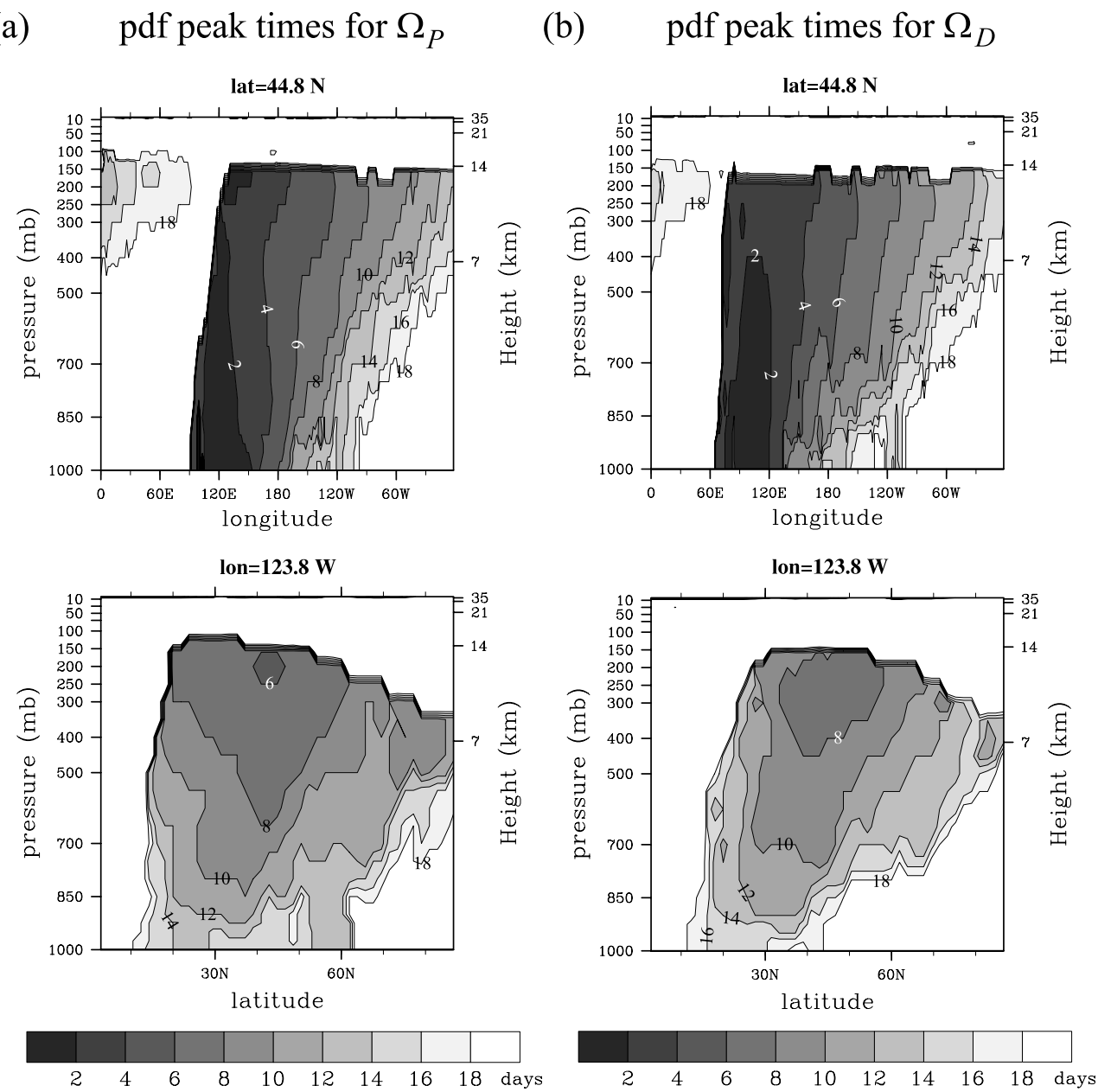


**Figure 6.** (a) Vertical structure of the peak time in days of the springtime ensemble average, $\langle \mathcal{G}(\xi) \rangle$, for $\Omega_P$. The top panel shows a constant-latitude cut at 44.8°N. The bottom panel shows a constant longitude cut at 123.8°W. (b) As in Figure 6a, but for $\Omega_D$. (c) As in Figure 6a, but for $\Omega_F$.

transport event of 14 April 2001, identified by an Asian dust cloud over the PNW region, does fall above the 90th percentile of the $\Omega_D$ burden for $\tau \geq 9$ days, but not as the most unusual day in terms of transport alone. While east Asian pollutants were observed in the PNW during 13–15 April 2001 [*Jaffe et al.*, 2003; *Price et al.*, 2003], Figures 8a and 8b show that long-range transport to the PNW was unusual only from the dust region, and not from the pollution region for which 14 April does not appear above the 90th percentile. The percentiles of the 14 April, $\Omega_P$ burdens of ages $\tau = 4$ to 12 days are 27, 62, 67, 75, 73, 76, 77, 75, and 72%, respectively. Thus the $\Omega_P$ burdens for 14 April are certainly above average for $\tau \geq 5$ days but not nearly as exceptional as the corresponding $\Omega_D$ burdens.

[30] Figure 9 shows the histograms of $[\widetilde{g}]_{PNW}$ for the $\Omega_P$ and $\Omega_D$ cases and $\tau = 8$ days to quantify to what degree events above the 90th percentile are outliers of their sample distribution. For $\Omega_D$, $[\widetilde{g}]_{PNW}$ is distributed over smaller values, with lower median and percentiles, as expected from the smaller area of $\Omega_D$. The histogram for the $\Omega_F$ case cannot be usefully compared at the same value of $\tau$ because of the slower $\Omega_F$-to-PNW transport. However, at $\tau \simeq 10$ days, the histogram for $\Omega_F$ (not shown) is qualitatively similar. For both $\Omega_P$ and $\Omega_D$, the event of late April 1998 lies in the extreme tail of the sample distribution. The April 2001 event, which for $\tau = 8$ days just barely lies above the 90th percentile of the distribution for $\Omega_D$, does not fall in the far tail of that distribution. This suggests that the April 2001

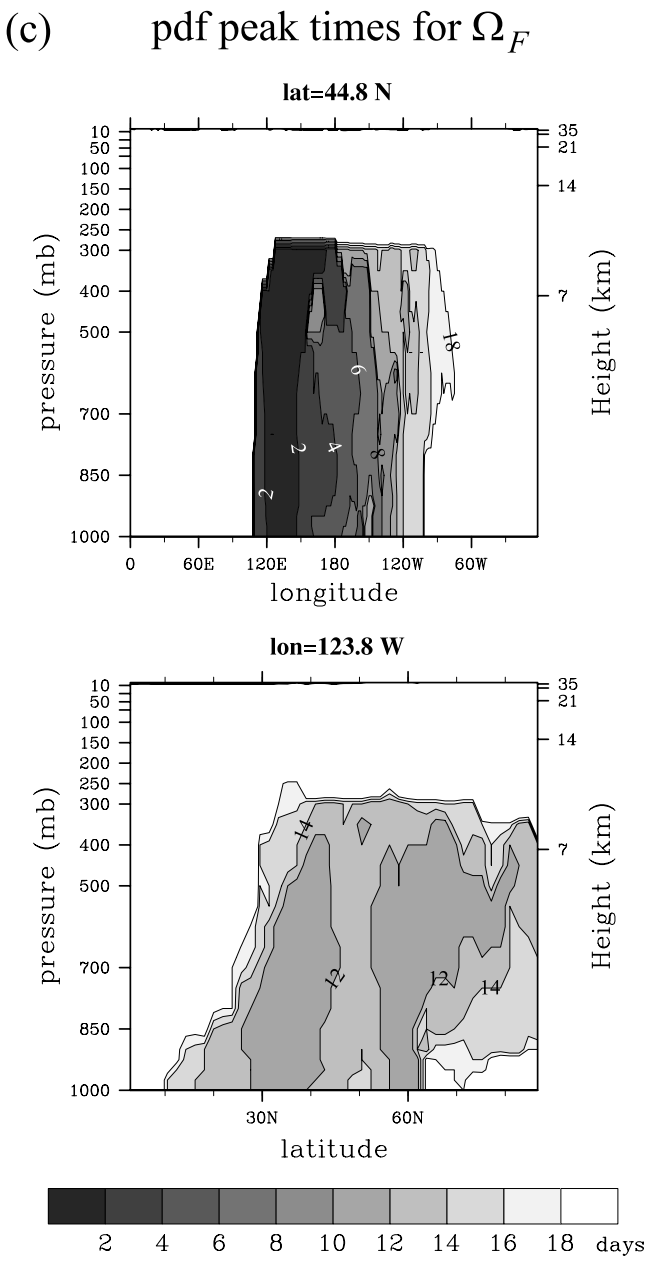


**Figure 6.** (continued)

event was observed as being spectacular in the PNW at least in part because of a large source event: the dust storm that labeled the $\Omega_D$-air with observable tracer.

[31] Because events correspond to outliers of the distribution of $\tilde{g}$ averaged over the PNW field-point region, we expect some sensitivity of the event identification to the definition of field-point region. To estimate this sensitivity, we considered transport from $\Omega_P$ to two additional field-point regions (not shown): The Pacific west (PW) box obtained by extending the southern edge of the PNW box south to 34.3°N, and the Pacific southwest (PSW) box obtained by shifting the original PNW box south by 9.5°. There is significant overlap between the PNW and PW events, but the detailed ranking of days above the 90th percentile differs, and days that do not appear for the PNW appear for the PW and vice versa. For example, 19980426 (using YYYYMMDD format) remains above the 95th percentile for the PW, but is displaced from rank 1 by 19990413 for $\tau = 9$, 10, and 11. Also, 20010414 now shows as an event for the PW at about the 95th percentile. Even for the PSW, there is still overlap with the PNW events, but with more reordering of the ranking. For the PSW, 20000423 and 20010414 share ranks 1 and 2, while 19980426/27 now appear between the 90th and 95th percentiles. For all three regions (PNW, PW, and PSW), the days clustered around 19990410 appear above the 95th percentile. The fact that different field-point regions experience different transport events, or the same events with different rankings of the Ω-air burden, reflects the fact that the structure of the Ω-air plume is highly variable and depends of the details of the flow.

[32] While well-known observed transport events clearly emerge from this analysis, other days that fall above the 90th percentile did not correspond to observed events. There are at least two reasons for this. First, the Ω air must carry a measurable tracer such as dust or a chemical

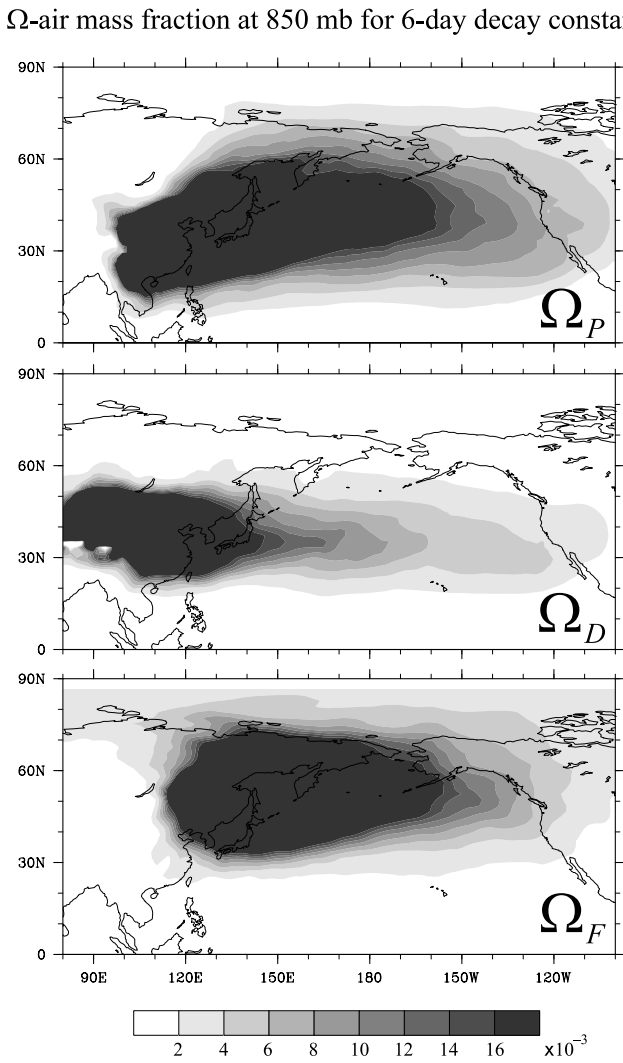


**Figure 7.** Springtime climatological air-mass fraction, $f(\tau_c)$, at 850 mb bearing a chemical signature from the contact region Ω indicated, assuming that the chemical has a decay time of $\tau_c = 6$ days.

a

Transport Events: $\Omega_P$ Air

| rank | τ = 4 days | 5 days | 6 days | 7 days | 8 days | 9 days | 10 days | 11 days | 12 days |
|---|---|---|---|---|---|---|---|---|---|
| 1 | 19990413 | 19980426 | 19980426 | 19980426 | 19980426 | 19980426 | 19980426 | 19980426 | 19980426 |
| 2 | 20010423 | 20010423 | 20010423 | 20010423 | 19990329 | 19970503 | 19990412 | 19990412 | 19990412 |
| 3 | 19990414 | 19990414 | 19990412 | 19970503 | 19970503 | 19990412 | 19970503 | 19970503 | 20000416 |
| 4 | 19980419 | 19990412 | 19970503 | 19990329 | 19990412 | 19990411 | 19990411 | 19990411 | 19970503 |
| 5 | 19990412 | 19990413 | 19990413 | 19990412 | 20010423 | 19980427 | 19980427 | 20010423 | 19990411 |
| 6 | 20000330 | 19980419 | 19990414 | 19980427 | 19980427 | 20010423 | 20010510 | 20010424 | 20010424 |
| 7 | 19990411 | 19970510 | 20010510 | 19990414 | 19990410 | 20010510 | 20010424 | 19980427 | 19970510 |
| 8 | 20000421 | 20010510 | 20000330 | 19990413 | 19990413 | 19990413 | 20010423 | 19970510 | 20010510 |
| 9 | 19990405 | 19970507 | 19990410 | 20010510 | 19990411 | 20010424 | 19990413 | 20010510 | 20010423 |
| 10 | 20000422 | 20000330 | 19970510 | 19990410 | 20010510 | 19990410 | 19970510 | 20000416 | 19980427 |
| 11 | 19970510 | 19970503 | 19980419 | 19990411 | 20010424 | 19970510 | 19990410 | 19970504 | 19970505 |
| 12 | 19980417 | 20000422 | 20000406 | 19970510 | 19990414 | 20010428 | 20010428 | 19990413 | 20010428 |
| 13 | 19980418 | 20000405 | 20010424 | 20010401 | 19970510 | 19990414 | 19970504 | 20010428 | 19990410 |
| 14 | 19970419 | 20000421 | 20000405 | 20010424 | 20010428 | 20000406 | 19990407 | 19990410 | 19970504 |
| 15 | 20010406 | 19990411 | 19970329 | 20000406 | 20010401 | 19990407 | 20000406 | 19990407 | 20000406 |
| 16 | 19970507 | 19990405 | 19970507 | 20000330 | 20000406 | 19990405 | 19990414 | 19970505 | 19990407 |
| 17 | 20010509 | 20010424 | 20010406 | 20010428 | 19990405 | 19970504 | 20000416 | 20000406 | 19990413 |
| 18 | 19980426 | 19970329 | 20000422 | 19980419 | 19970418 | 19970418 | 19970505 | 19990414 | 19970507 |
| 19 | 20000423 | 20000329 | 19970418 | 20010331 | 20000330 | 20010401 | 20000425 | 20000405 | 19990414 |
| 20 | 19980425 | 19980418 | 20010331 | 19990405 | 20000405 | 20000330 | 20000405 | 20000422 | 20000422 |
| 21 | 19970418 | 19980417 | 19980427 | 20000405 | 20010331 | 20000405 | 19970418 | | |
| 22 | 20010510 | 19970418 | 20010401 | 19970418 | 20010406 | | | N=200 | N=195 |
| 23 | 19970404 | 20010406 | 19990411 | | | N=210 | N=205 | | |
| 24 | 19970417 | | | N=220 | N=215 | | | | |
| | | N=230 | N=225 | | | | | | |
| | N=235 | | | | | | | | |

**Figure 8.** (a) Dates in YYYYMMDD format for which the PNW-box-averaged $\Omega_P$-air mass burden aged $\tau$ days or less, $[\widetilde{g}(\mathbf{r}, t|\Omega_P,\tau)]_{PNW}$, falls above its 90th percentile. Observed transport events [e.g., *Jaffe et al.*, 2003] and dates contiguous with these are shaded. The dates are sorted in descending order (the indicated rank) according to the corresponding value of $[\widetilde{g}(\mathbf{r}, t|\Omega_P,\tau)]_{PNW}$. The sample size available for each $\tau$ is given by $N$. (b) As in Figure 8a, but for $\Omega_D$. (c) As in Figure 8a, but for $\Omega_F$.

pollutant that has survived for at least time $\tau$. If the $\Omega$ air is clean from the beginning, or by the time it arrives in the field-point region, then there is nothing measurable to label it with its origin. Second, someone must actually be taking measurements in the field-point region (using, e.g., mid-tropospheric LIDAR or aircraft) at the time of a transport event. However, the point of our analysis is not verification of a transport model with observations. By using the tracer-independent transport diagnostic, $\mathcal{G}$, we are able to distinguish pure transport events from "pollution events" at the source. For example, we can now answer the question: Do we see Asian pollutants and dust in unusually high concentrations merely because there was an unusually large source, or because there was unusually nondispersive transport from the pollution region to the point of observation? For those events that emerge as unusual from this analysis, transport played a crucial role. Furthermore, our analysis quantitatively assigns "ages" to the fluid elements of $\Omega$ origin, which should be of value to the interpretation of chemical analyses of observed pollutants.

## 7. Physical Conditions for Long-Range Transport

[33] As a first step in identifying the structure of the flow that is effective in bringing $\Omega$ air to the PNW box, we study time-lagged correlations between the winds (horizontal velocity) and the PNW-averaged, vertically integrated $\mathcal{G}$. The idea is to identify flow structures resulting in a transit-time pdf that is particularly large over the PNW for a fixed transit time $\xi = t - t'$. To that end we consider the one-dimensional time series of daily averages

$$\psi(t, \xi, \Omega) = \left[\widetilde{\mathcal{G}}(\mathbf{r}, t|\Omega, t - \xi)\right]_{PNW}, \tag{8}$$

for fixed $\xi$. To calculate correlations between $\psi$ and other fields, we use $\hat{\psi}$ obtained from $\psi$ by "standardizing" it, that is, by removing its mean and dividing by its variance. Flow anomaly structures emerge from the time-lagged correlation

$$\mathcal{V}(\mathbf{r}, \xi, \tau) \equiv \left\langle \mathbf{v}(\mathbf{r}, t - \tau)\, \hat{\psi}(t, \xi, \Omega) \right\rangle, \tag{9}$$

where $\mathbf{v}(\mathbf{r}, t - \tau)$ is the horizontal fluid velocity $\tau \leq \xi$ days earlier than $t$. Note that the mean flow, $\langle \mathbf{v} \rangle$, does not contribute to $\mathcal{V}$ since $\langle \hat{\psi} \rangle = 0$, so that $\langle \mathbf{v}\hat{\psi} \rangle = \langle \mathbf{v}'\hat{\psi} \rangle$, where $\mathbf{v}' \equiv \mathbf{v} - \langle \mathbf{v} \rangle$. To estimate where on average the $\Omega$-air burden of age $\xi - \tau$ deviates from its climatological mean $\tau$ days prior to a fluctuation in $\hat{\psi}$, we calculate the time-lagged correlation between $\hat{\psi}$ and $\mathcal{G}$ itself:

$$\Gamma(\mathbf{r}, \xi, \tau) \equiv \left\langle \widetilde{\mathcal{G}}(\mathbf{r}, t - \tau|\Omega, t - \xi)\, \hat{\psi}(t, \xi, \Omega) \right\rangle. \tag{10}$$

[34] The correlation $\mathcal{V}$ is essentially a weighted average of $\mathbf{v}'$, with a weight proportional to the fluctuations of $\psi$

b Transport Events: $\Omega_D$ Air

| rank | τ = 4 days | 5 days | 6 days | 7 days | 8 days | 9 days | 10 days | 11 days | 12 days |
|---|---|---|---|---|---|---|---|---|---|
| 1 | 19980425 | 19980425 | 19980426 | 19980426 | 19980426 | 19980426 | 19980426 | 19980426 | 19980426 |
| 2 | 20010509 | 19980419 | 19980425 | 19980425 | 20010510 | 20010510 | 20010510 | 20010510 | 20010510 |
| 3 | 19990413 | 20010509 | 19980419 | 19970510 | 19970510 | 20010509 | 20010509 | 20010509 | 20010509 |
| 4 | 20000330 | 19980426 | 20010509 | 20010509 | 19980425 | 19980427 | 19980427 | 19970510 | 19970510 |
| 5 | 19970504 | 19980508 | 19980508 | 20010510 | 19980427 | 19970510 | 19970510 | 19980427 | 19980427 |
| 6 | 19990406 | 20000502 | 20010510 | 19980427 | 20010509 | 19980425 | 19980425 | 19980425 | 20010506 |
| 7 | 19980508 | 19970507 | 20000502 | 19980508 | 19970503 | 20000502 | 20010506 | 20010506 | 19980425 |
| 8 | 19980418 | 19990413 | 19970507 | 19980419 | 19970508 | 20010505 | 20000502 | 20000502 | 20000502 |
| 9 | 19990414 | 19990414 | 20000503 | 19970508 | 19980508 | 19970508 | 20010505 | 20000503 | 20000503 |
| 10 | 19980426 | 20000423 | 19980509 | 20000503 | 20010508 | 19970503 | 20000503 | 20010505 | 19990407 |
| 11 | 19990327 | 20010510 | 19990413 | 20000502 | 20000502 | 20000503 | 20010414 | 19990407 | 20010505 |
| 12 | 20010505 | 20000330 | 20000423 | 19970507 | 19980419 | 20010508 | 19970508 | 19970503 | 19970508 |
| 13 | 20010510 | 20000405 | 19970508 | 20010427 | 19970507 | 20010506 | 19990407 | 19970508 | 19970503 |
| 14 | 19990502 | 19980509 | 20010427 | 19980509 | 20000503 | 19970507 | 19970503 | 20010414 | 20010414 |
| 15 | 19980507 | 19970504 | 19970510 | 19970503 | 19980509 | 20010414 | 20010508 | 19980428 | 19980428 |
| 16 | 19980419 | 20010429 | 19990414 | 20010423 | 20010505 | 19980419 | 19970507 | 20010508 | 20010508 |
| 17 | 20010430 | 19980503 | 20000405 | 19990414 | 20010423 | 20010423 | 19980428 | 20010415 | 20010423 |
| 18 | 20000502 | 20010427 | 20010423 | 19990413 | 20010427 | 19990407 | 20010423 | 20010423 | 20010415 |
| 19 | 19990401 | 19990406 | 19980420 | 20000423 | 19990414 | 19980508 | 20010427 | 19970507 | 19970507 |
| 20 | 19970403 | 19990328 | 19970502 | 19980510 | 19990413 | 20010427 | 20010415 | 20010427 | 19980430 |
| 21 | 20010429 | 19990503 | 19970505 | 20000405 | 19980510 | 19980509 | 19980419 | | |
| 22 | 19990412 | 19990425 | 20010429 | 20010505 | 20010413 | | | N=200 | N=195 |
| 23 | 19990328 | 19970404 | 19980503 | | | N=210 | N=205 | | |
| 24 | 19980509 | | | N=220 | N=215 | | | | |
| | | N=230 | N=225 | | | | | | |
| | N=235 | | | | | | | | |

c Transport Events: $\Omega_F$ Air

| rank | τ = 4 days | 5 days | 6 days | 7 days | 8 days | 9 days | 10 days | 11 days | 12 days |
|---|---|---|---|---|---|---|---|---|---|
| 1 | 19970429 | 19970429 | 19980327 | 19980328 | 19990329 | 19990330 | 20010429 | 20010429 | 19970421 |
| 2 | 19980419 | 19970430 | 19990329 | 19990329 | 19990330 | 20010429 | 19990331 | 19970504 | 19980411 |
| 3 | 19970430 | 19970328 | 19970429 | 19970328 | 19970430 | 19990331 | 19970504 | 19980411 | 19990503 |
| 4 | 20000507 | 19970502 | 19970328 | 19990330 | 19970329 | 19970430 | 19970503 | 20010430 | 19970504 |
| 5 | 19980508 | 19980419 | 19970430 | 19970430 | 19970503 | 20010428 | 20010430 | 19970421 | 20010429 |
| 6 | 19980420 | 20010430 | 19970502 | 19970429 | 19970429 | 19970503 | 20010428 | 19970503 | 19970503 |
| 7 | 19970502 | 19980509 | 19990328 | 19970329 | 19980408 | 19970504 | 19970430 | 19990503 | 20010430 |
| 8 | 19980509 | 20000507 | 19970329 | 19990328 | 20000406 | 20010430 | 19980411 | 20010428 | 20010428 |
| 9 | 19970501 | 19990328 | 20010430 | 19970503 | 20000407 | 19980408 | 19980408 | 19990401 | 19990403 |
| 10 | 19980421 | 19990329 | 19980509 | 19970502 | 19970504 | 19990403 | 19990401 | 19970430 | 20010407 |
| 11 | 19980413 | 19980420 | 20000406 | 20000406 | 20010428 | 20000407 | 19990403 | 19990403 | 19970430 |
| 12 | 19990504 | 19970501 | 19980419 | 19980408 | 19980329 | 19970429 | 19990503 | 19980408 | 19990405 |
| 13 | 20010502 | 19980422 | 19970501 | 20010430 | 20010429 | 19970501 | 19970501 | 19990404 | 20010502 |
| 14 | 20010430 | 19980508 | 19970503 | 20000407 | 20010430 | 19970502 | 19970502 | 19970502 | 19980412 |
| 15 | 19990503 | 20010505 | 19980413 | 19980419 | 19970502 | 20000406 | 19990404 | 19990405 | 19990404 |
| 16 | 20010505 | 19970329 | 20000507 | 19980413 | 19990331 | 19980409 | 19980409 | 19980409 | 19970422 |
| 17 | 19980412 | 19980408 | 19980422 | 19980509 | 19980409 | 19990503 | 19970429 | 19970501 | 19970506 |
| 18 | 19970507 | 19980421 | 20010506 | 19970501 | 19970501 | 19990401 | 20000407 | 19970506 | 19980408 |
| 19 | 19970428 | 19980413 | 20000331 | 20010428 | 19970330 | 19970330 | 19970421 | 19980410 | 19980410 |
| 20 | 19970328 | 20000406 | 20010505 | 19980422 | 19990403 | 20010502 | 20000406 | 19970429 | 20010406 |
| 21 | 20000506 | 19990504 | 19980420 | 19980424 | 20010502 | 19980410 | 19970506 | | |
| 22 | 19980507 | 19970503 | 19980408 | 19970330 | 19980413 | | | N=200 | N=195 |
| 23 | 20010406 | 19980412 | 19980504 | | | N=210 | N=205 | | |
| 24 | 20010429 | | | N=220 | N=215 | | | | |
| | | N=230 | N=225 | | | | | | |
| | N=235 | | | | | | | | |

**Figure 8.** (continued)

from its mean value. Thus both negative and positive fluctuations (less than and more than average $\Omega_P$ air over the PNW) contribute to $\mathcal{V}$. However, if we write $\hat{\psi} = \hat{\psi}^+ + \hat{\psi}^-$, where $\hat{\psi}^+ = \hat{\psi}$, if $\hat{\psi} > 0$, and $\hat{\psi}^+ = 0$ otherwise, we find that $\langle \mathbf{v}'\hat{\psi} \rangle = \langle \mathbf{v}'\hat{\psi}^+ \rangle + \langle \mathbf{v}'\hat{\psi}^- \rangle$ is dominated by $\langle \mathbf{v}'\hat{\psi}^+ \rangle$. Thus $\mathcal{V}$ is essentially a composite of those flow perturbations that result in a large value of $\psi$ a time $\tau$ later. The correlation $\Gamma$ is similarly dominated by $\langle \widetilde{\mathcal{G}}\hat{\psi}^+ \rangle$ so that, $\tau$ days prior to a positive excursion of $\hat{\psi}$, $\widetilde{\mathcal{G}}$ is on average greater than $\langle \widetilde{\mathcal{G}} \rangle$ where $\Gamma > 0$, and $\widetilde{\mathcal{G}}$ is on average less than $\langle \widetilde{\mathcal{G}} \rangle$ where $\Gamma < 0$

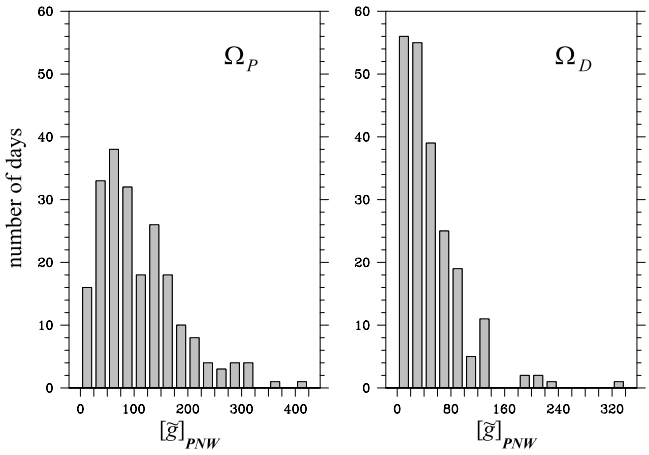


**Figure 9.** Histograms of the PNW-box-averaged burden, $[\widetilde{g}]_{PNW}$, of $\Omega_P$ and $\Omega_D$ air aged 8 days or less in units of kg m$^{-2}$. In these units, the 90th and 95th percentiles of $[\widetilde{g}]_{PNW}$ are 204 and 266 for $\Omega_P$, and 101 and 134 for $\Omega_D$. The corresponding median values of $[\widetilde{g}]_{PNW}$, representative of the climatological background, are 92.2 and 38.2 for $\Omega_P$ and $\Omega_D$, respectively.

(anticorrelation with $\hat{\psi}$). We continue our analysis in terms of $\mathcal{V}$ instead of $\langle \mathbf{v}'\hat{\psi}^+ \rangle$, because $\mathcal{V}$ contains the information we seek and additionally has the conventional interpretation as the regression coefficient in the statistical "model" $\mathbf{v}(\mathbf{r}, t - \tau) = \mathcal{V}(\mathbf{r}, \xi, \tau)\ \hat{\psi}(t)$. (Note that $\Gamma$ and $\mathcal{V}$ are correlations, or linear regression coefficients, and not Pearson's correlation coefficient $-1 \le r \le 1$.)

[35] Because of its importance as a steady source of industrial pollution, we restrict our analysis here to transport from $\Omega_P$. Figure 10 shows the mean flow, $\langle \mathbf{v} \rangle$, together with the correlations $\mathcal{V}$ and $\Gamma$ for $\xi = 7$ days, and time lags $\tau$ ranging from the field time back to the source time. For Figure 10, the ensemble averages $\langle \ldots \rangle$ of equations (9) and (10) have been computed over all five springs of simulation to ensure good statistics. The corresponding $\psi$ has been standardized with its 5-spring mean and variance. (Calculating the ensemble average separately for each spring, using $\psi$ standardized with the mean and variance of each spring, and then averaging the 5 correlations, results in only small differences with no changes in the qualitative patterns. Also, increasing $\xi$ from 7 to 9 days does not change the qualitative picture.) The correlation $\mathcal{V}$ is shown at 300 mb, where the transport of $\Omega_P$ air is most rapid (see Figures 4 and 6a). The correlation patterns are very similar at 500 mb. The statistical significance of the correlations has been estimated from the standard t-statistic (not shown). The discussion below will focus on the regions where $\Gamma$ exceeds $\sim$4 kg m$^{-2}$ day$^{-1}$, and the t-statistic there exceeds its thresholds for the 95% significance level. The evolution of $\Gamma$ with $\tau$ (or, equivalently, with time since last $\Omega_P$ contact, $\xi - \tau$) stands in sharp contrast to the climatological average behavior of $\widetilde{\mathcal{G}}$ visible in Figure 3. The latter is an average over all realized evolutions of $\mathcal{G}$, while the correlations $\Gamma$ and $\mathcal{V}$ represent the evolution of perturbations from the climatological means that correspond to favorable $\Omega$-to-PNW transport.

[36] The correlation patterns $\Gamma$ and $\mathcal{V}$ are not very sensitive to the definition of the PNW field-point region. Extending the southern boundary of the PNW box south to 34.3°N has a small quantitative impact on the correlations without changing their qualitative character. Shifting the entire PNW box south by 9.5° results in a more zonal $\mathcal{V}$ throughout the $\Gamma > 0$ regions for $\tau \lesssim 4$ days, which for $\tau = 0$ points into the now more southerly field-point box.

[37] Detailed examination of the transport for individual years shows that there is considerable interannual variability in the trans-Pacific springtime transport. Five simulated springs are insufficient to attempt a statistical analysis of this interannual variability. However, to give an idea of its character, we show in Figure 11 the correlations $\Gamma$ and $\mathcal{V}$ computed separately for each spring at the field time ($\tau = 0$). While the overall feature of a flow anomaly steering $\Omega_P$ air across the PNW box is common to all springs, the correlation patterns vary significantly from year to year. Part of the interannual variability of the flow is likely due to El Niño/Southern Oscillation (ENSO), which is known to have an effect on upper tropospheric flow including jet-stream position and structure [see, e.g., *Yang et al.*, 2002]. A convenient measure of the phase and amplitude of ENSO is the southern oscillation index (SOI). (The SOI is defined in terms of the monthly-mean mean-sea level pressure difference, $\Delta p$, between Tahiti and Darwin as SOI $\equiv 10 \times (\Delta p - \overline{\Delta p})/\sigma(\Delta p)$, where $\overline{\Delta p}$ is the long-time average of $\Delta p$ and $\sigma(\Delta p)$ is the corresponding standard deviation.) A sustained negative (positive) SOI indicates an El Niño (La Niña) episode. The March-April-May average SOI for 1997 to 2001 had the values $-15.7$, $-17.5$, $+9.6$, $+9.9$, and $-0.7$, respectively (see, e.g., the online SOI archive http://www.bom.gov.au/climate/current/soihtm1.shtml of the Bureau of Meteorology, Australia, 2003).

[38] The correlation $\mathcal{V}$ suggests teleconnections of the PNW, $\Omega_P$-air fraction with flow not only in regions of $\Gamma > 0$ (light shading), but also elsewhere. However, here our focus is on $\mathcal{V}$ in regions where $\Gamma$ exceeds $\sim$4 kg m$^{-2}$ day$^{-1}$, a convenient threshold for locating where the $\Omega_P$-air burden significantly exceeds its climatological mean $\tau$ days prior to a large $\Omega_P$-air fraction over the PNW. Figure 10 then suggests the following average scenario of favorable $\Omega_P$-to-PNW transport: A strengthened east Asian jet [e.g., *Yang et al.*, 2002] carries $\Omega_P$ air off the Asian continent about one day after $\Omega_P$ contact ($\tau \sim 6$ days). About 3 days after $\Omega_P$ contact ($\tau \sim 4$ days), $\mathcal{V}$ again indicates strengthened westerly flow over the western Pacific. After the $\Omega_P$ air is over the central North Pacific ($\tau \sim 2$ days), transport events tend to correspond to subsequent southeast transport between counter-rotating flow perturbations and stretching along the strain axes (computed but not shown) in the outflow region of the perturbation field. Examination of the correlations for the individual years for $\tau = 2$ days (not shown) shows that this correlation pattern is dominated by the negative-SOI springs, with a much more zonal flow perturbation in the region of positive $\Gamma$ for 1999 and 2000. Finally, Figures 10 and 11 show that during the field day ($\tau = 0$), anticyclonic flow perturbations centered on the western United States steer $\Omega_P$ air across the PNW. Simultaneously, the outflow region of the perturbation for

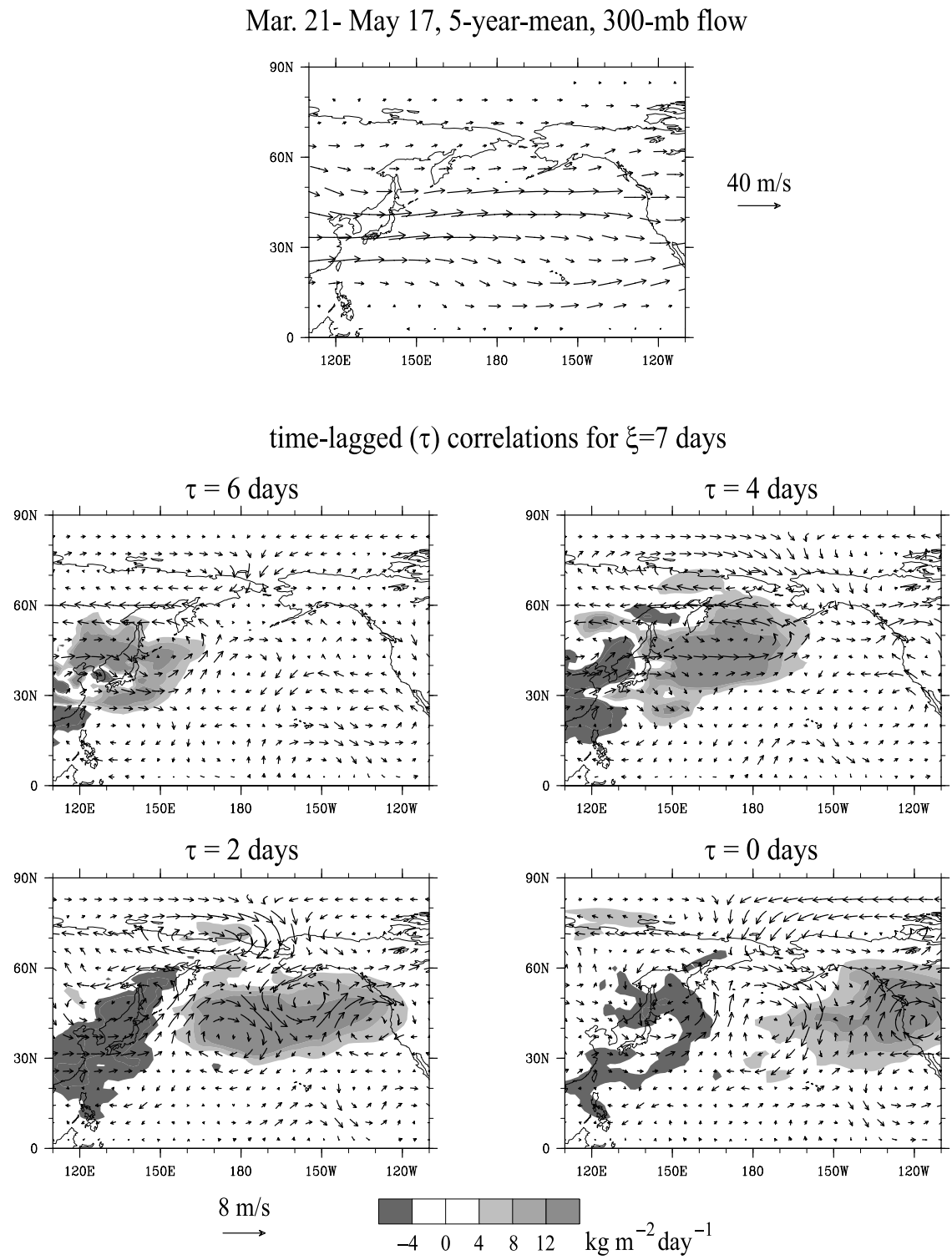


**Figure 10.** Top panel: 21-March-to-17-May, 5-year-mean flow at 300 mb. Bottom panels: Correlations shown are $\mathcal{V}$ (vectors) and $\Gamma$ (shading). $\mathcal{V}$ is the time lagged correlation between $[\tilde{\mathcal{G}}]_{PNW}$ at a fixed transit time of $\xi = 7$ days and the horizontal velocity a time $\tau$ earlier. $\Gamma$ is the corresponding correlation between $[\tilde{\mathcal{G}}]_{PNW}$ and $\tilde{\mathcal{G}}$ itself. The ensemble for the correlation here includes all available data of the 5 springs simulated. Note that the mean flow and $\mathcal{V}$ have different vector scales.

$\tau = 2$ days, which survives as a more southwesterly flow anomaly for $\tau = 0$, tends to pool $\Omega_P$ air over the subtropical central Pacific. This is particularly visible for the negative-SOI springs.

[39] We emphasize that we are not describing the evolution of $\Omega$ air for any particular transport event, but rather the evolution of perturbations of $\tilde{\mathcal{G}}$ and **v** from their means that correlate with changes in the fraction of $\Omega$ air of age $\xi$ days

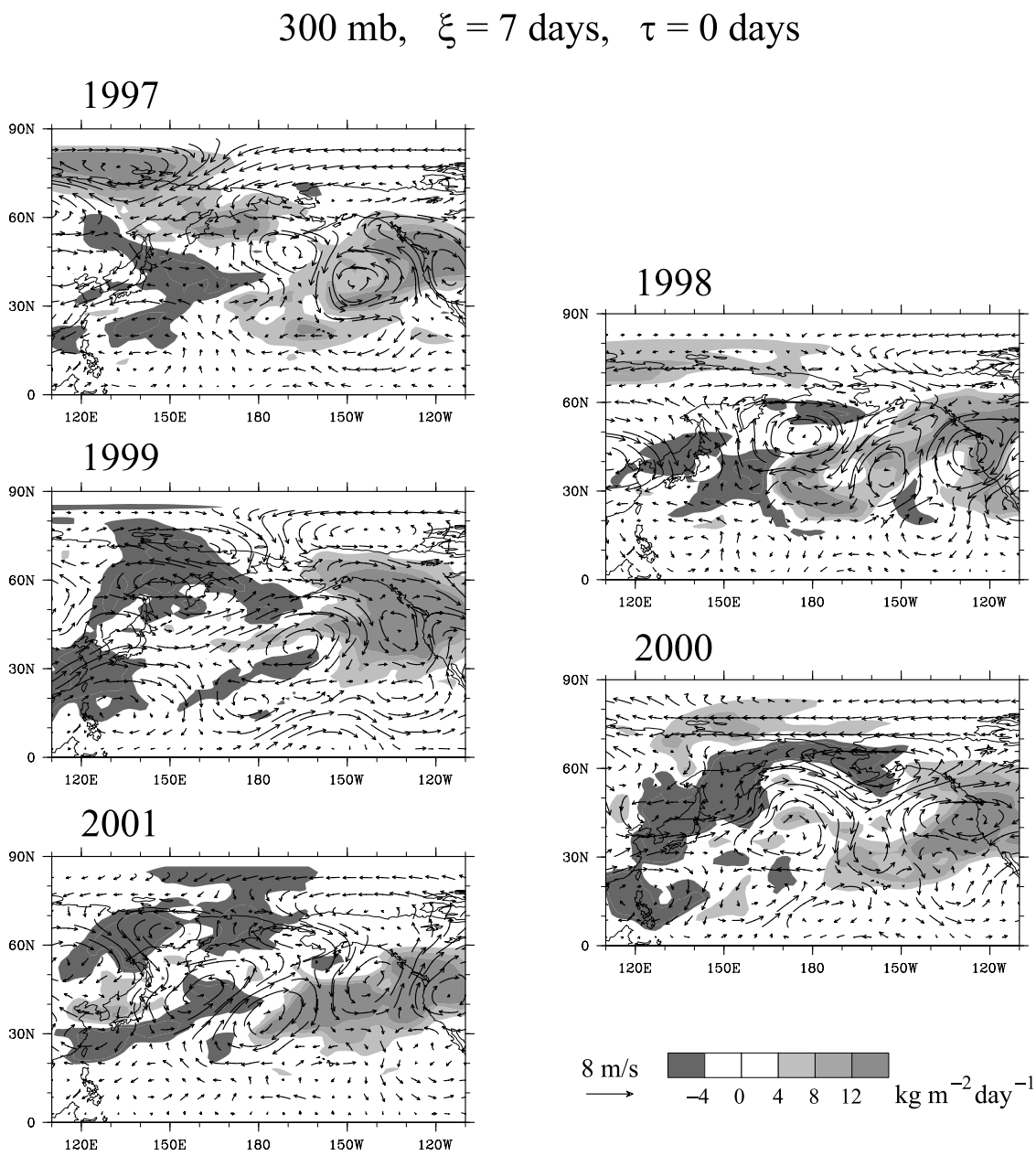


**Figure 11.** Time-lagged correlations $\Gamma$ and $\mathcal{V}$ as in Figure 10, but for individual years and for $\tau = 0$, only.

in the PNW box. These correlation patterns are dominated by positive fluctuations of $\hat{\psi}$ (including transport events) and therefore indicate the average flow and burden anomalies that correspond to favorable transport to the PNW.

## 8. Summary and Conclusions

[40] This paper has set out to establish the climatological springtime transport from three east Asian regions, $\Omega$ (Figure 1a), and to establish the statistics of transport events to the Pacific Northwest (PNW) region of North America (Figure 1b). We focused on a tracer-independent transport diagnostic, the transit-time pdf, $\mathcal{G}$, to isolate the role of transport from other processes such as chemistry and deposition. Using the MATCH transport model [*Rasch et al.*, 1997], we have constructed the springtime transport climatology of daily averages of the transit-time pdf, $\mathcal{G}(\mathbf{r}, t|\Omega, t')$ for an ensemble of 51 source days, $t'$, per spring (21 March to 10 May) for the five years, 1997 to 2001.

[41] The climatological mean transport from the dust and pollution regions is qualitatively similar, with rapid access to the middle and upper troposphere and transport across the Pacific that is dominated by upper tropospheric flow. Over the west coast of North America, the average transit-time pdfs peak around 8 days in the upper troposphere and about 6 days later at the surface. The average transport from the Siberian fire region to the North American coast occurs in the lower troposphere with pdf-peak times of 12–14 days with only weak vertical gradients. The transport climate has been characterized here by the mean state of $\mathcal{G}$, that is, by

the mean plume of $\Omega$ air per age interval. A full characterization of the variability of $\mathcal{G}$ about this mean will be given elsewhere.

[42] We identified transport events to the PNW as those days for which the vertically integrated fraction of $\Omega$ air of age $\tau$ or less falls in the tail of its sample distribution. Days for which this fraction falls above its 90th percentile include well-documented transport events, as well as days that seem to have gone unnoticed observationally. For the PNW, the late-April event of 1998 is the largest, most unusual event of the five springs studied. We concentrated on the PNW region for the analysis of events because of the availability of a number of observations and for economy of presentation. However, from our simulations it is just as straightforward to perform an event analysis for any other point or region, such as the southwestern United States, or even Hawaii on the southern edge of the climatological "plume" of $\Omega_P$ and $\Omega_D$ air. Because events are outliers of a distribution, and the precise structure of the $\Omega$-air plume depends on details of the flow, event identification is sensitive to the definition of field-point region. An analysis of $\Omega_P$-air transport events for the southwestern United States identified 23 April 2000 and 14 April 2001 as the two most unusual springtime events.

[43] As a first step in identifying flow resulting in favorable transport to the PNW region, we studied time-lagged correlations between velocity and $[\widetilde{\mathcal{G}}]_{PNW}$, the PNW-box-integrated transit-time pdf at a fixed transit time. This allowed us to identify the average conditions and pathways that bring more than average $\Omega$ air to the PNW. The transport of east Asian air for particular events can be highly nonzonal in a rough zig-zag pattern: up to the North Pacific, then downward to the subtropical Pacific, followed by northwesterly transport to the PNW, often with a pool remaining behind in the tropics. Although the correlations between $[\widetilde{\mathcal{G}}]_{PNW}$ and $\widetilde{\mathcal{G}}$ show that on average there is a more zonal progression, the correlations between $[\widetilde{\mathcal{G}}]_{PNW}$ and the velocity preserve this approximate zig-zag pattern. Correlations of the $\Omega$-air burden over the field-point region with transport processes in the vicinity of the source region, such as convective fluxes (parameterized in MATCH) and frontal lifting, remain to be explored.

[44] Although spring has received considerable attention because of its spectacular, easily observable dust events, there must also be a climatological transport of air from east Asia during other seasons, with the potential of carrying industrial pollutants to North America. The sample distribution of the $\Omega$-air fraction of a certain age will define transport events for other seasons. Summer events may potentially be important because they would add to greater air-pollution problems in North America.

[45] Interannual variability and the role of ENSO are fascinating aspects of long-range transport that need to be addressed with a much larger multiyear data set than was available here. A study involving several decades could be feasible by going from daily to monthly timescales allowing for much more economical monthlong mixing-ratio pulses. (Interannual variability of transport events, however, would still require much shorter pulses.)

[46] We focused on three east Asian contact regions that contain particularly important sources of pollutants and particulates for trans-Pacific transport to western North America. However, any given air parcel will also contain fluid elements that had contact with other surface regions. For example, pollutants of European origin are known to contribute to the composition of air over the north Pacific and over western North America [*Newell and Evans*, 2000; *Jaeglé et al.*, 2003]. By extending the transit-time pdf for a given contact patch, $\Omega$, to a propagator of geographically distributed surface boundary conditions [*Holzer and Hall*, 2000], one can compute the joint pdf of transit time and place of origin. Such an approach has recently been applied to stationary oceanic transport by *Haine and Hall* [2002]. While impractical on a daily timescale, in a future study we hope to calculate the climatological transport on multiday timescales from contiguous contact patches tiling the entire Northern Hemisphere.

[47] During the formal revision stage of this paper, we became aware of the study by *Stohl et al.* [2002], who used a global Lagrangian particle dispersal model for a one-year simulation of passive tracers emitted with a CO source pattern. By tagging the particles with release time, the authors construct seasonal mean "age spectra," which are conceptually related to the transit-time pdfs calculated here. For trans-Pacific transport, our studies are in broad agreement in terms of timescales and spatial structures.

[48] Finally, we consider this study to be an illustration of the kind of information that is available from daily averages of the transit-time pdf. Because $\mathcal{G}$ has the natural interpretation as a distribution of times since last contact with a source region, the transit-time-pdf approach should be valuable to the interpretation of tropospheric chemistry. Particularly fruitful may be an analysis of the long-range transport of light hydrocarbons whose chemistry may be represented by simple exponential decay [e.g., *Ehhalt et al.*, 1998].

[49] **Acknowledgments.** This work was supported by CFCAS grant GR-021. We thank Tim Hall for discussions and comments on the manuscript, Phil Austin, Henryk Modzelewski, and Roland Stull for discussions and generous computing support, Terry Clarke for pointing out the reference on forest-fire simulations, and the anonymous reviewers for their comments.

## References

Benkovitz, C. M., M. T. Scholtz, J. Pacyna, L. Tarrason, J. Dignon, E. C. Voldner, P. A. Spiro, J. A. Logan, and T. E. Graedel, Global gridded inventories of anthropogenic emissions of sulfur and nitrogen, *J. Geophys. Res.*, *101*, 29,239–29,253, 1996.

Berntsen, T. K., S. Karlsdottir, and D. A. Jaffe, Influence of Asian emissions on the composition of air reaching the northwestern United States, *Geophys. Res. Lett.*, *26*, 2171–2174, 1999.

DeFries, R. S., and J. R. G. Townshend, NDVI-derived land cover classification at a global scale, *Int. J. Remote Sens.*, *15*, 3567–3586, 1994.

Duncan, B. N., R. V. Martin, A. C. Staudt, R. Yevich, and J. A. Logan, Interannual and seasonal variability of biomass burning emissions constrained by satellite observations, *J. Geophys. Res.*, *108*(D2), 4100, 10.1029/2002JD002378, 2003.

Ehhalt, D. H., F. Rohrer, A. Wahner, M. J. Prather, and D. R. Blake, On the use of hydrocarbons for the determination of tropospheric OH concentrations, *J. Geophys. Res.*, *103*, 18,981–18,997, 1998.

Gong, S. L., X. Y. Zhang, T. L. Zhao, I. G. McKendry, D. A. Jaffe, and N. M. Lu, Characterization of soil dust aerosol in China and its transport and distribution during 2001 Ace-Asia: 2. Model simulation and validation, *J. Geophys. Res.*, *108*(D9), 4262, doi:10.1029/2002JD002633, 2003.

Hacker, J. P., I. G. McKendry, and R. B. Stull, Modeled downward transport of a passive tracer over western North America during an Asian dust event in April 1998, *J. Appl. Meteorol*, *40*, 1617–1628, 2001.

Haine, T. W. N., and T. M. Hall, A generalized transport theory: Water-mass composition and age, *J. Phys. Oceanogr.*, *32*, 1932–1946, 2002.

Hall, T. M., and M. Holzer, Advective-diffusive mass flux and implications for stratosphere-troposphere exchange, *Geophys. Res. Lett.*, *30*(5), 1222, doi:10.1029/2002GL016419, 2003.

Hall, T. M., and R. A. Plumb, Age as a diagnostic of stratospheric transport, *J. Geophys. Res.*, *99*, 1059–1070, 1994.

Heald, C. L., et al., Asian outflow and trans-Pacific transport of carbon monoxide and ozone pollution: An integrated satellite, aircraft, and model perspective, *J. Geophys. Res.*, *108*, doi:10.1029/2003JD003507, in press, 2003.

Holzer, M., Analysis of passive tracer transport as modeled by an atmospheric general circulation model, *J. Clim.*, *12*, 1659–1684, 1999.

Holzer, M., and T. M. Hall, Transit-time and tracer-age distributions in geophysical flows, *J. Atmos. Sci.*, *57*, 3539–3558, 2000.

Husar, R. B., et al., Asian dust events of April 1998, *J. Geophys. Res*, *106*, 18,317–18,330, 2001.

Jacob, D. J., J. A. Logan, and P. P. Murti, Effect of rising Asian emissions on surface ozone in the United States, *Geophys. Res. Lett.*, *26*, 2175–2178, 1999.

Jacob, D. J., et al., Transport and Chemical Evolution over the Pacific (TRACE-P) aircraft mission: Design, execution, and first results, *J. Geophys. Res.*, *108*(D20), 8781, doi:10.1029/2002JD003276, 2003.

Jaeglé, L., D. A. Jaffe, H. U. Price, P. Weiss-Penzias, P. I. Palmer, M. J. Evans, D. J. Jacob, and I. Bey, Sources and budgets for CO and $O_3$ in the northeastern Pacific during the spring of 2001: Results from the PHOBEA-II Experiment, *J. Geophys. Res.*, *108*(D20), 8802, doi:10.1029/2002JD003121, 2003.

Jaffe, D., et al., Transport of Asian air pollution to North America, *Geophys. Res. Lett.*, *26*, 711–714, 1999.

Jaffe, D. A., T. Anderson, D. Covert, B. Trost, J. Danielson, W. Simpson, D. Blake, J. Harris, and D. Streets, Observations of ozone and related species in the northeast Pacific during the PHOBEA campaigns: 1. Ground based observations at Cheeka Peak, *J. Geophys. Res.*, *106*, 7449–7461, 2001.

Jaffe, D., I. G. McKendry, T. Anderson, and H. Price, Six "new" episodes of trans-Pacific transport of air pollutants, *Atmos. Environ.*, *37*, 391–404, 2003.

Kajii, Y., et al., Boreal forest fires in Siberia in 1998: Estimation of area burned and emissions of pollutants by advanced very high resolution radiometer satellite data, *J. Geophys. Res.*, *107*(D24), 4745, doi:10.1029/2001JD001078, 2002.

Kalnay, E., et al., The NMC/NCAR 40-year reanalysis project, *Bull. Am. Meteorol. Soc.*, *77*, 437–471, 1996.

Kistler, R., et al., The NCEP/NCAR 50-year reanalysis, *Bull. Am. Meteorol. Soc.*, *82*, 247–267, 2001.

Kotchenruther, R. A., D. A. Jaffe, H. J. Beine, T. L. Anderson, J. W. Bottenheim, J. M. Harris, D. R. Blake, and R. Schmitt, Observations of ozone and related species in the northeast Pacific during the PHOBEA campaigns: 2. Airborne observations, *J. Geophys. Res.*, *106*, 7463–7483, 2001.

McKendry, I. G., J. P. Hacker, R. Stull, S. Sakiyama, D. Mignacca, and K. Reid, Long-range transport of Asian dust to the Lower Fraser Valley, British Columbia, Canada, *J. Geophys. Res.*, *106*, 18,361–18,370, 2001.

Merrill, J. T., M. Uematsu, and R. Bleck, Meteorological analysis of long-range transport of mineral aerosols over the North Pacific, *J. Geophys. Res.*, *94*, 8584–8598, 1989.

Morse, P. M., and H. Feshbach, *Methods of Theoretical Physics*, 997 pp., McGraw-Hill, New York, 1953.

Newell, R. E., and M. J. Evans, Seasonal changes in pollutant transport to the North Pacific: The relative importance of Asian and European sources, *Geophys. Res. Lett.*, *27*, 2509–2512, 2000.

Price, H. U., D. A. Jaffe, P. V. Doskey, I. McKendry, and T. Anderson, Vertical profiles of $O_3$, aerosols, CO and NMHCs in the northeast Pacific during the TRACE-P and ACE-ASIA experiments, *J. Geophys. Res.*, *108*(D20), 8799, doi:10.1029/2002JD002930, 2003.

Prospero, J. M., P. Ginoux, O. Torres, S. E. Nicholson, and T. E. Gill, Environmental characterization of global sources of atmospheric soil dust identified with the Nimbus 7 Total Ozone Mapping Spectrometer (TOMS) absorbing aerosol product, *Rev. Geophys.*, *40*(1), 1002, doi:10.1029/2000RG000095, 2002.

Rasch, P. J., and M. Lawrence, Recent developments in transport methods at NCAR, in *MPI Workshop on Conservative Transport Schemes*, MPI Rep. 265, pp. 65–75, Max Planck Inst. for Meteorol., Hamburg, Germany, 1998.

Rasch, P. J., N. M. Mahowald, and B. E. Eaton, Representations of transport, convection and the hydrologic cycle in chemical transport models: Implications for the modeling of short lived and soluble species, *J. Geophys. Res.*, *102*, 28,127–28,138, 1997.

Stohl, A., A one-year Lagrangian "climatology" of airstreams in the northern hemisphere troposphere and lowermost stratosphere, *J. Geophys. Res.*, *106*, 7263–7279, 2001.

Stohl, A., S. Eckhardt, C. Forster, P. James, and N. Spichtinger, On the pathways and timescales of intercontinental air pollution transport, *J. Geophys. Res.*, *107*(D23), 4648, doi:10.1029/2001JD001396, 2002.

Tratt, D. M., R. J. Frouin, and D. L. Westphal, April 1998 Asian dust event: A southern California perspective, *J. Geophys. Res.*, *106*, 18,371–18,379, 2001.

Uno, I., H. Amano, S. Emori, K. Kinoshita, I. Matsui, and N. Sugimoto, Trans-Pacific yellow sand transport observed in April 1998: A numerical simulation, *J. Geophys. Res.*, *106*, 18,331–18,344, 2001.

Vaughan, J. K., C. Claiborn, and D. Finn, April 1998 Asian dust event over the Columbia Plateau, *J. Geophys. Res.*, *106*, 18,381–18,402, 2001.

Wotawa, G., and M. Trainer, The influence of Canadian forest fires on pollutant concentrations in the United States, *Science*, *288*, 324–328, 2000.

Yang, S., K.-M. Lau, and K.-M. Kim, Variations of the east Asian jet stream and Asian-Pacific-American winter climate anomalies, *J. Clim.*, *15*, 306–325, 2002.

Yienger, J. J., M. Galanter, T. A. Holloway, M. J. Phadnis, S. K. Guttikunda, G. R. Carmichael, W. J. Moxim, and H. Levy II, Episodic nature of air pollution transport from Asia to North America, *J. Geophys. Res.*, *105*, 26,931–26,945, 2000.

Zhao, T. L., S .L. Gong, X. Y. Zhang, and I. G. McKendry, Modeled size-segregated wet and dry deposition budgets of soil dust aerosol during ACE-Asia 2001: Implications for trans-Pacific transport, *J. Geophys. Res.*, *108*(D23), 8665, doi:10.1029/2002JD003363, 2003.

M. Holzer, Department of Earth and Ocean Sciences, University of British Columbia, 6339 Stores Road, Vancouver, British Columbia, Canada V6T 1Z4. (mholzer@eos.ubc.ca)

D. A. Jaffe, Interdisciplinary Arts and Sciences, University of Washington–Bothell, 22011 26th Avenue SE, Bothell, WA 98021, USA. (djaffe@u.washington.edu)

I. G. McKendry, Department of Geography, University of British Columbia, 250-1984 West Mall, Vancouver, British Columbia, Canada V6T 1Z2. (ian@geog.ubc.ca)